INVESTIGATION OF POLYVINYL ALCOHOL ADDED WITH CALCINED MUSSEL SHELL BIOCOMPOSITE

TIANG MING WAI

A project report submitted in partial fulfilment of the requirements for the award of Bachelor of Engineering (Honours) Chemical Engineering

Lee Kong Chian Faculty of Engineering and Science
Universiti Tunku Abdul Rahman

April 2020

DECLARATION

I hereby declare that this project report is based on my original work except for citations and quotations which have been duly acknowledged. I also declare that it has not been previously and concurrently submitted for any other degree or award at UTAR or other institutions.

Signature   :

Name   :   TIANG MING WAI

ID No.   :   15UEB02421

Date   :   15/05/2020

APPROVAL FOR SUBMISSION

I certify that this project report entitled **"INVESTIGATION OF POLYVINYL ALCOHOL ADDED WITH CALCINED MUSSEL SHELL BIOCOMPOSITE"** was prepared by **TIANG MING WAI** has met the required standard for submission in partial fulfilment of the requirements for the award of Bachelor of Engineering (Honours) Chemical Engineering at Universiti Tunku Abdul Rahman.

Approved by,

Signature :

Supervisor : Ir Dr Bee Soo Tueen

Date : 15/05/2020

ACKNOWLEDGEMENTS

ABSTRACT

This study is to investigate the characteristics of polyvinyl alcohol (PVOH) added with different amount of calcined mussel shell (HAp). HAp was extracted from the shell of *Perna viridis* through thermal calcination and followed by solution casting method to produce PVOH composite films, consisting 0 phr to 5 phr calcined mussel shell. The tensile strength of the PVOH composites increases upon added with 2 phr calcined mussel shell then decreases when amount of calcined mussel shell increases to 4 phr. For the Young's modulus, it has similar trend as the tensile strength whereas addition of small amount of calcined mussel shell could provide the reinforcement effect while decreased in interfacial adhesion effect due to the agglomeration at high loading level of calcined mussel shell. The elongation at break of the PVOH composites was increased when the amount of calcined mussel shell added increased. For scanning electron microscopy, cavities can be observed in the PVOH composites with less amount of calcined mussel shell while flake like structure can be observed in PVOH composites with greater amount of calcined mussel shell. For X-ray diffraction analysis, the peak broadening effect indicates a decrease in HAp crystallite size which has ruptured and well dispersed within PVOH matrix. Addition of calcined mussel shell into PVOH matrix had weaken the water absorption capability of PVOH composites. In fourier transform infrared spectroscopy analysis, the significant peaks occurred approximately at 3254 cm^{-1} and 2940 cm^{-1}, indicating the presence of O-H group bonding and C-H bonding respectively. Besides that, the strength of hydrogen bonding in the PVOH composites had increased as the amount of calcined mussel shell increased.

TABLE OF CONTENTS

CHAPTER

LIST OF TABLES

LIST OF FIGURES

LIST OF SYMBOLS / ABBREVIATIONS

b	FWHM, radian
d	d-spacing, Å
k	Scherrer Constant
Ca	Calcium
O	Oxygen
λ	wavelength, nm
PVOH	Polyvinyl alcohol
HAp	Hydroxyapatite
CES	Calcined eggshell
SEM	Scanning Electron Microscopy
XRD	X-ray Diffraction
FTIR	Fourier Transform Infrared Spectroscopy
DSC	Differential Scanning Calorimetry
TGA	Thermogravimetric Analysis
EDX	Energy Dispersive X-ray Spectroscopy
phr	parts per hundred resins
rpm	revolutions per minute

CHAPTER 1

INTRODUCTION

1.1   Background

In recent years, the polymeric materials have become an indispensable part of people's lives and its demand is increasing year by year. Besides that, there are various types of synthetic polymers are being manufactured for different purposes or applications over the past century, such as packaging, electronic, 3D printing, medical devices etc. Since there is a huge segment of polymers are petroleum-based and they are non-biodegradable, the disposition of the polymer wastes has become a significant environmental issue. However, this detrimental environmental impact can be mitigated by alternatives materials which are biodegradable polymers proposed by scientists and researchers while the biodegradable polymers are widely used in various applications and able to replace the non-biodegradable polymers (Abhilash and Thomas, 2017).

A biodegradable polymer can be defined as material which able to degrade completely when exposed to the microorganisms, enzymes, aerobic or anaerobic processes while its physical and chemical characteristics deteriorate during the degradation process (Abhilash and Thomas, 2017). Over past 50 years, biodegradable polymers had received significant attention and being applied to substitute some materials, such as metal and wood. The biodegradable polymers can be categorized simply as natural polymers and synthetic polymers, where natural polymers are synthesized from biomass or plant while synthetic polymers are derived from non-renewable resources such as petroleum or natural gas (Luyt and Malik, 2019).

The biodegradable polymers lost their durability and toughness properties in return able to be biodegradable. As a result, one or more composite materials can be added into the polymers to intensify the mechanical strength and other properties. The composite polymers can be composed of matrix and dispersed phases where the dispersed phase is usually embedded in matrix to act as reinforcement (Jose and Joseph, 2012). With the development of technology, the biodegradable polymer composites have started to be applied to medical

field such as medical implants and tissue-engineered products to help healing or tissue repair (Zhang *et al.*, 2014).

Polyvinyl alcohol (PVOH) is one of the biodegradable polymers which has been applied in the biomedical applications due to its biocompatibility, non-toxic, non-carcinogenic and non-immunogenic properties (Paradossi, Cavalieri and Chiessi, 2003; Aramwit *et al.*, 2010). PVOH hydrogels had been invented for artificial tissue such as artificial heart lining, soft contact lens, articular cartilage, artificial skin and pancreas membrane (Hassan, C.M., Peppas, 2000). On the other hand, the bio-inertness of PVOH implant causing it does not adhere to tissue and it has poor mechanical strength at the same time. In this case, hydroxyapatite (HAp) has been added into PVOH and play a role of composite material which can improves the bioactivities, osteoconductivity and mechanical properties of PVOH (Pan and Xiong, 2009; Liu, Chen and Zhou, 2010). Hydroxyapatite is able to be synthesized or extracted from the natural sources which include cuttlefish bones (Rocha *et al.*, 2005), eggshells, land snails (Macha *et al.*, 2015) and nacreous materials (Lemos *et al.*, 2006).

1.2 Problem Statements

Polyvinyl alcohol (PVOH) is a biodegradable polymer which has properties of water soluble, no odour and non-toxic, making it widely used in textiles and papermaking industries, coating agent for food supplements or food packaging and it also can be used for pharmaceutical and biomedical applications. On the other hand, the hydroxyapatite (HAp) which is responsible for strength and stiffness of bone is found in the mussel shell waste and can be used to improve the mechanical properties of PVOH. Utilizing mussel shell waste not only able to mitigate the impact to the environment, but also help bone recovery. Therefore, this research has provided an opportunity to study the effects of calcined mussel shell in polyvinyl alcohol composites. In this study, the changes in properties of polyvinyl alcohol composites are observed by adding certain amount of calcined mussel shell into polyvinyl alcohol composites. The problem statements for this study were identified as the following:

1. What are the effects of HAp in PVOH composite in terms of mechanical properties, surface morphologies and crystallinity?

2. What are the effects of HAp in PVOH composite in terms of chemical structure?

1.3   Aim and Objectives

This study aims to examine the characterization of polyvinyl alcohol added with different loading levels of calcined mussel shell composite. The study of effect includes the morphology of composite, bonding interaction, as well as mechanical properties. The main objective was divided into the following sub-objectives:

1. To investigate the mechanical properties of PVOH composite with different amount of HAp composition.
2. To investigate the surface morphologies and crystallinity of PVOH composite with different amount of HAp composition.

1.4   Scope of Study

This research was subjected into three stages, which were preparation of HAp, preparation of HAp-PVOH composites and samples characterization.

1.4.1   Mechanical Properties

Tensile test was conducted to determine the force required to break a specimen and the extent of the specimen when stretched or elongated to its breaking point by the stress and strain. The tensile test for the specimen film was carried out according to ASTM D882 standard to measure the tensile strength, Young's modulus and elongation at break.

1.4.2   Morphologies

The morphology of polyvinyl alcohol composite was determined by using scanning electron microscopy (SEM).

1.4.3   Crystallinity

X-ray diffraction (XRD) analysis was conducted to determine the crystalline structure for both calcined mussel shell and polyvinyl alcohol composite.

1.4.4   Chemical Interactions of Bonding

Fourier transform infrared (FTIR) was used to identify the chemical features and shifts that occur due to the addition of HAp into polyvinyl alcohol. The interaction of bonding between two functional groups of the composite could be studied by using FTIR.

1.4.5   Water Absorption Test

The water absorption test was conducted to determine the amount of water that able to be absorbed by the polyvinyl alcohol-hydroxyapatite composites.

1.5   Summary

There are lot of other segment which included the literature review, methodology, work plan, results, discussion, conclusion and recommendations will be discussed in the following chapters.

CHAPTER 2

LITERATURE REVIEW

2.1   Polyvinyl Alcohol

2.1.1   Properties of Polyvinyl Alcohol

Polyvinyl alcohol (PVOH) is a colourless hydrophilic polymer with hydroxyl group attached on each repeating unit where the chemical structure was showed in Figure 2.1, it can be produced by complete or partial hydrolysis of polyvinyl acetate with water or methanol (Zaaba, Ismail and Mariatti, 2016) (Gooch, 2007). PVOH has some excellent properties, such as semi-crystalline, biodegradable, nontoxic and biocompatible. PVOH has been widely applied in various applications which including textile coatings, packaging films, adhesives, biomedical and pharmaceutical applications due to its outstanding properties (Thomas *et al.*, 2018).
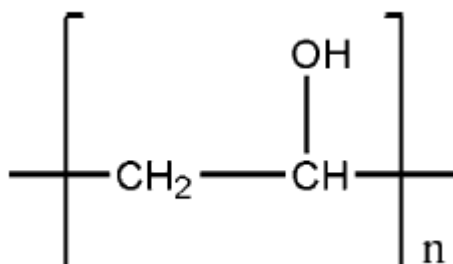
Figure 2.1 Structure of Polyvinyl Alcohol (PVOH) (Gooch, 2007)

The solubility and crystallizability of PVOH are depending on the degree of hydrolysis, thus there are two categories of PVOH, partially hydrolysed polyvinyl alcohol and fully hydrolysed polyvinyl alcohol. There is a copolymer will appear in the PVOH which is the polyvinyl acetate (PVAc). The hydrogen bonding of the hydroxyl groups are weaken due to the presence of the hydrophobic acetate groups which has not been hydrolysed (Hassan, C.M., Peppas, 2000). The fully hydrolysed PVOH has higher degree of crystallinity which will form smaller crystalline and leads to better mechanical properties,

water resistance and lower liquids and gases permeability (Tretinnikov and Zagorskaya, 2012).

2.1.2   Applications of Polyvinyl Alcohol

Because of the outstanding properties of polyvinyl alcohol, such as resistance to organic solvents, water soluble, biodegradable, nontoxic and biocompatible, thus it had been applied in numerous biomedical and pharmaceutical fields (Thomas *et al.*, 2018). For instance, drug delivery systems, wound dressings, artificial grafts, cartilage tissue engineering and contact lenses. In addition, cross-linking hydrogen bonds or hydroxyl groups of PVOH physically or chemically would results in the improvement of mechanical strength and stability in biological environment (Syed, Garg and Sarkar, 2018) (Barui, 2018).

Moreover, polyvinyl alcohol can be synthesized in the form of film or fiber and used for various purposes such as textile and paper sizing, coatings, binders, food packaging, laminating adhesives and protective colloid in suspension polymerization (Rudnik, 2012) .

2.2   Green Mussel

2.2.1   Introduction of Green Mussel

Green mussel, *Perna viridis*, also known as the Asian green mussel or Philippine green mussel. it generally ranges from 80 to 100 millimetres in length and has an elongate shell. The colour of the outer shell is in dark brownish green while the interior shell has an iridescent pale bluish green sheen (Siriwardena, 2018).

The native range of *Perna viridis* is along the tropical waters of the Indo-Pacific. However, due to its fast growth and strong adaptability to the environmental variables, it had been introduced to the Caribbean, Australia, Japan and North and South America (Siriwardena, 2018). It able to transport to new regions by attaching itself to the hull of ships or it was larvae in the sea water ballast tanks of ships (Gobin *et al.*, 2013).

2.2.2   Impact of Green Mussel

Because of the fast growth and strong adaptability of green mussel, the biodiversity is potentially affected by the invasion of the green mussel. For

example, the oyster may die and replaced by green mussel (Siriwardena, 2018). On the other hand, massive consumption of mussels produces the aquaculture by-product shells and lead to a significant solid waste problem. However, the mussel shells waste are able to be utilized as the bio-filler for polymer matrices (Fombuena *et al.*, 2014).

2.2.3 Composition of Green Mussel Shell

The composition of the green mussel shell is shown in Table 2.1. It contains highest concentration of calcium (Ca) element and CHO is representing the carbon, hydrogen, oxygen and nitrogen (Sangwaranatee *et al.*, 2018).

Table 2.1: Compositions of *Perna viridis* Shell (Sangwaranatee *et al.*, 2018)

Element	Concentration (Wt%)
CHO	68.064
Ca	31.528
Sr	0.155
P	0.052
Fe	0.043
Mn	0.002

2.2.4 Applications of Mussel Shell

There were over 1 million tonnes of mussel shell waste being produced every year worldwide and lead to serious solid waste problem. From a study conducted by Martínez-García *et al.* (2017) stated that the mussel shell can be used as an aggregate or filler in concrete or mortar. Furthermore, the mussel shell also has been applied to remove the phosphorus and heavy metal from the contaminated water. The study carried by Ji *et al.*, (2019) stated that the mussel shell can be used for removal of nitrogen and phosphorus from the eutrophic wastewater.

2.3 Hydroxyapatite (HAp)

2.3.1 Introduction of Hydroxyapatite

Hydroxyapatite (HAp) has a chemical formula of $Ca_{10}(PO_4)_6(OH)_2$, it is a mineral form of calcium apatite and main mineral constituent of bones. HAp is the hydroxyl end member of the complex apatite group and has hexagonal

crystal system (Rigano and Lionetti, 2016). HAp is a biodegradable, biocompatible and osteoconductive material, thus it is suitable to be used for bone regeneration, bone tissue engineering and medical devices (Trakoolwannachai, Kheolamai and Ummartyotin, 2019). Besides that, HAp also can be applied to the dental and orthopaedic implants (Wakai, 2013).

2.3.2   Synthesis of Hydroxyapatite

Hydroxyapatite can be synthesized from various sources, including fish bones, bovine bones, egg shells, cuttlefish bones, coral and sea shells (Macha *et al.*, 2015). In addition, there are several methods or techniques have been used to synthesis the HAp, for instance, wet precipitation, hydrothermal, electrochemical deposition, biomimetic deposition, multiple emulsion and sol-gel approach (Sathiyavimal *et al.*, 2019).

Wet precipitation is the most common method to produce hydroxyapatite, it requires orthophosphoric acid (H_3PO_4) to react with the calcium hydroxide ($Ca(OH)_2$). The equation for the chemical reaction is shown in equation 1.

$$10Ca(OH)_2 + 6H_3PO_4 \rightarrow Ca_{10}(PO_4)_6(OH)_2 + 18H_2O \qquad (1)$$
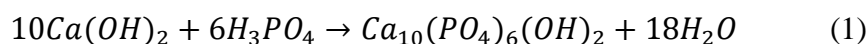
(Mazumder *et al.*, 2018)

On the other hand, HAp also can be synthesized through the sol-gel approach which involved drying and calcination at temperature up to 900℃. According to the study of Mondal *et al.* (2019), they managed to yield HAp from the Tuna bones with calcination at 1000℃ for 1 hour.

2.3.3   Application of Hydroxyapatite Composites

Hydroxyapatite has been implemented in biomedical applications including scaffold fabrication for bone replacement, artificial graft, dental and orthopaedic implants and drug delivery (Mondal *et al.*, 2019) due to its high similarity and biocompatible between hydroxyapatite and bones (Chen *et al.*, 2019). However, the pure HAp has poor mechanical properties such as low fatigue strength and brittleness, and consequently limit the application as medical material (Trakoolwannachai, Kheolamai and Ummartyotin, 2019). Therefore, in order to

enhance the mechanical properties of HAp, it usually combines with different synthetic polymers to produce the hydroxyapatite composites. Addition of HAp also increased the bioactivity of the polymer (Mazumder *et al.*, 2018).

Apart from this, HAp has been applied in removal and recovery of heavy metal ions such as lead, nickel, zinc, cobalt, copper, uranium and cadmium when it binds with chitosan or other polymers to produce hydroxyapatite composite (Gupta, Kushwaha and Chattopadhyaya, 2012).

2.4   Tensile Test

2.4.1   Background of Tensile Test

Tensile test is conducted to determine the tensile properties which are one of the indicators to ensure the quality in most of the material specifications. The tensile test is able to provide some important mechanical properties, including tensile strength, modulus of elasticity, elongation, yield strength, yield point and other properties (Rahman and Zhafer Firdaus Syed Putra, 2018). The tensile test measures the force required to break a specimen and the extension which the specimen elongates to its breaking point (Saba, Jawaid and Sultan, 2018). The tensile properties are measured when developing a new material and the results of tensile test could be referred when selecting materials for engineering applications (Davis, 2004).

Simple stress-strain test is applied for the determination of some of the mechanical parameters for various polymeric materials, such as tensile and yield strength, modulus of elasticity and elongation at break. The specimen is subjected to the tension force and the elongation of specimen is recorded as the tension force increases gradually. The stress-strain curve can be plotted by converting the force-elongation data into engineering stress and strain (Callister and Rethwisch, 2010).

2.4.2   Tensile Strength

Tensile strength can be defined as the maximum stress that the specimen able to sustain before it breaks or fractures. In other words, it is the maximum tensile stress that the material can take before fracture. The tensile strength can be

obtained from the stress-strain curve, since it is the stress at maximum on the curve (Callister and Rethwisch, 2008).

2.4.3   Young's Modulus

Young's modulus also known as elastic modulus, it measures the stiffness or resistance to elastic deformation of a material, the stiffer materials will result in greater modulus. It can be defined as the ratio of stress to strain as shown in equation 2.

$$E = \frac{\sigma}{\epsilon}$$

(2)

(Callister and Rethwisch, 2008)

2.4.4   Elongation at Break

Ductility is one of the important mechanical properties which can be expressed quantitatively as the percent elongation. Ductility is a measurement of the degree of plastic deformation sustained at break. A ductile material able to sustain more plastic deformation while brittle material is able to sustain very little or no plastic deformation. The percent elongation is defined as the percentage of plastic strain at fracture or

$$\%EL = \frac{l_f - l_o}{l_o} \times 100\%$$

(3)

Where l_f is the fracture length and l_o is the original length (Callister and Rethwisch, 2008).

2.5   Scanning Electron Microscopy (SEM)

2.5.1   Background of SEM

SEM is the technique that has been employed to observe and analyse the surface phenomena and microstructure characteristics of the solid materials. SEM has magnification up to 300,000 times and spatial resolution of 1 nm. It can provide several useful information such as morphology, topography, surface features, shape and size (Sharma *et al.*, 2018). SEM has been applied to wide range of

materials, including metals, polymers, membranes, ceramics and etcetera. The specimen used can be either in solid or powder form (Ul-Hamid, 2018).

The thermionic or field emission cathode is used in scanning electron microscope to accelerate the electrons with a voltage of 1 kV to 40 keV between the cathode and anode and direct them at the specimen. The electron beam is then demagnetized by magnetic field lenses and metal slits within vacuumed column to obtain a monochromatic beam with diameter lesser than 100 nm. The electron beam hits the surface of the specimen and loses energy, low energy electrons such as secondary electrons can escape from the surface of the specimen and detected to provide the surface information of the specimen (Sharma *et al.*, 2018).

2.5.2   Morphology

Morphology is a study of form including structure, shape and size which are significant for material research. The morphology of a nanostructured material is very important due to the form will dominates its physical and chemical properties. The shape of nanomaterials which is strongly correlated to its properties is gained by the interaction of size and molecular interactions during the self-assembling process. On the other hand, for nanocomposite, the properties are affected by the morphology of individual nanomaterials and nature of interactions which is determined by distribution of nanomaterials in the matrix (Sanyal, Datta and Hazra, 2007).

2.5.3   SEM/EDX

Energy dispersive X-ray spectroscopy (EDX) is a technique for identifying and quantifying elemental compositions in a specific sample. Specific wavelength of X-rays is emitted when the atoms on the surface of specimen are excited during bombardment by the electron beam from SEM. The emitted X-rays is analysed by an energy dispersive detector by measuring the number of the emitted X-rays versus their energy that is the characteristic of the chemical elements (Bergström, 2015).

2.6 X-ray Diffraction (XRD)

2.6.1 Background of XRD

XRD is being applied to study the characteristic of single crystal or polycrystalline materials. It is able to analyse the microstructure features of the material, including crystal structures, crystallographic orientations, phase identification, degree of crystallinity, strain, grain size and presence of imperfections (Rajeshkumar, Bharath and Geetha, 2019).

The X-ray radiation forms a beam and directed to the sample, the incident beam of X-rays will be partly absorbed, scattered and transmitted through the specimen. The interaction between the incident X-ray beam and electrons in the specimen causing the scattering and diffraction of X-ray. The constructive interference of monochromatic beam produces diffraction peaks, while the atomic positions within the lattice planes can be used to determine the peak intensities (Kohli, 2012).

2.6.2 Crystallinity

Crystallinity of a polymer can be defined as the degree as to which a region where polymer chains are aligned with each other or the fraction of the polymer which consists of regions showing three-dimensional order. A polymer with large degree of irregularity in polymer chains or little crystallinity is known as amorphous polymer (Crawford and Quinn, 2016).

The crystallinity of polymer is correlated with the presence of the branching in polymer chain. The branching reduces the density and crystallinity by prevent the polymer chain from packing close together. The degree of crystallinity of polymer directly affects the mechanical, chemical, thermal and optical properties of the materials (Riley, 2012).

2.7 Water Absorption Test

Water absorption is a limiting factors that could affects the mechanical properties of the composite materials and reduces its applicability. There are two types of water are being absorbed by the polymer which are free water and bound water. Water molecules that able to move through the void spaces freely

are known as free water, while the bound water are the water molecules that delimited to the polar groups of the polymers. The strength of water absorption in composite materials contingents on various factors, including temperature, porosity, diffusivity, exposed surface area and etcetera (Delgado and de Lima, 2018).

2.8   Fourier Transform Infrared Spectroscopy (FTIR)

Fourier transform infrared spectroscopy is a technique that has been widely used in material analysis in chemistry, biology and physics fields (McCluskey, 2016). It is able to determine bonding mechanisms of the materials through molecular vibrations which correlate with the symmetry of molecules. The wavelength of infrared radiation lies between 10 cm^{-1} and 10000 cm^{-1} or frequency of 10^{12} to 10^{14} Hz, which overlaps with frequency of the molecular vibrations. The infrared radiation is absorbed when it has same frequency as the molecular vibration and induce an excitation to higher energy state (Peak, 2013). The vibrational state of a molecule is changed due to the absorption of infrared radiation and being excited to higher energy state. The state transition will occur when it induces a dipole and the changes of electric dipole causing stretching and bending (Alawam, 2014).

2.9   Characterization Analysis of Calcined Eggshell

2.9.1   SEM Analysis of Calcined Eggshell

Figure 2.2 had showed the surface morphologies of the calcined eggshell (CES) powder at magnification of 1000X and 10,000X by using the scanning electron microscope. The irregular shape particles of CES with particles sizes of approximately 5 μm were highly crowded can be observed. The small particles size of CES could result in better dispersion in the PVOH composites due to its higher specific surface area (Bee *et al.*, 2017).

(a)   (b)
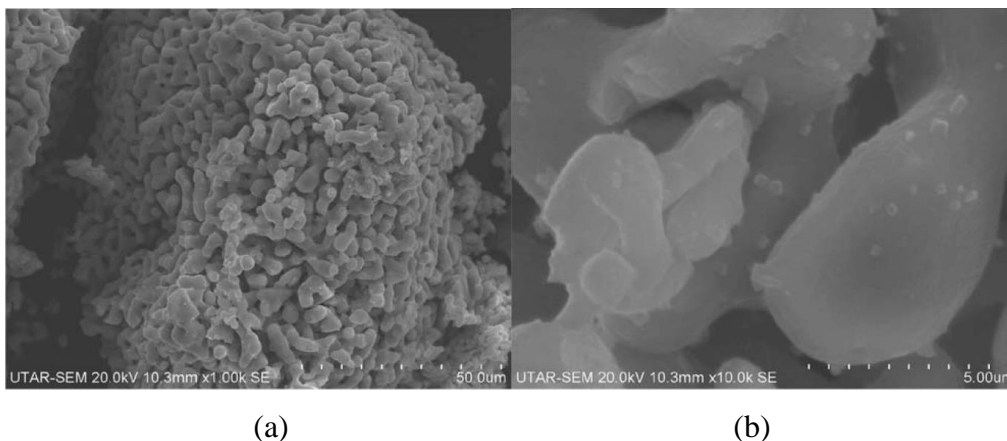
Figure 2.2 SEM micrographs of calcined eggshell powder at magnification of
(a) 1000 times and (b) 10,000 times (Bee *et al.*, 2017)

2.9.2   EDX Analysis of Calcined Eggshell

According to the Figure 2.3, the EDX analysis of the CES powder detected few
peaks which represented the calcium and the oxygen. The calcination of the
eggshell waste at high temperature would convert the main constituent eggshell
which is calcium carbonate ($CaCO_3$) into calcium oxide (CaO) and carbon
dioxide (CO_2), the chemical reaction as shown in equation below.

$$CaCO_3 \rightarrow CaO + CO_2 \tag{4}$$
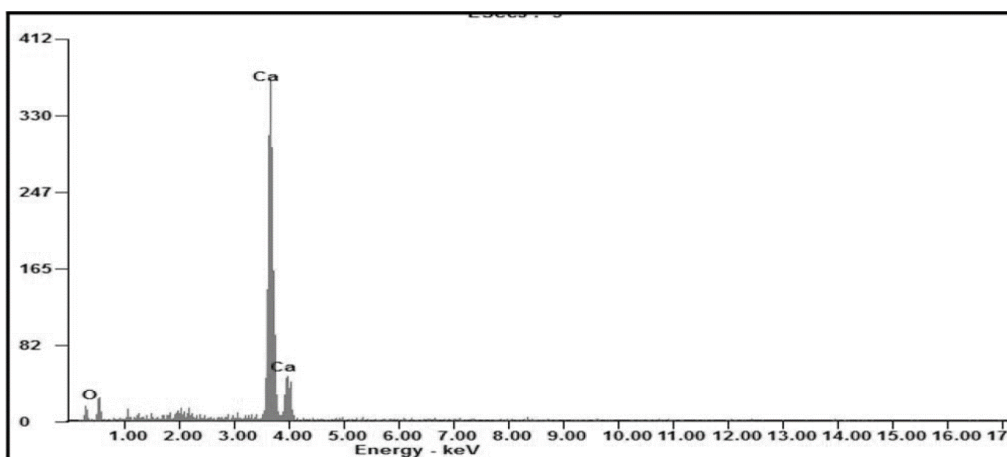
(Bee *et al.*, 2017)

Figure 2.3 Energy Spectra X-ray analysis result of calcined eggshell powder
(Bee *et al.*, 2017).

2.9.3   XRD Analysis of Calcined Eggshell

There were two deflection peaks occurred and detected at 2θ of about 32° and 38° in the XRD curve of CES powder as shown in Figure 2.4. In addition of that, the high crystallinity behaviour of pristine CES powder can be characterized by the straight baseline of the XRD curve. By referring to Figure 2.4, the crystallite sizes obtained from the two deflection peaks at 2θ of 32.328° and 37.480° were 601.55 Å and 627.07 Å respectively. Furthermore, the highly ordered arrangement of CES crystallite resulted in highly packed crystallites with small values of d and R (Bee *et al.*, 2017).
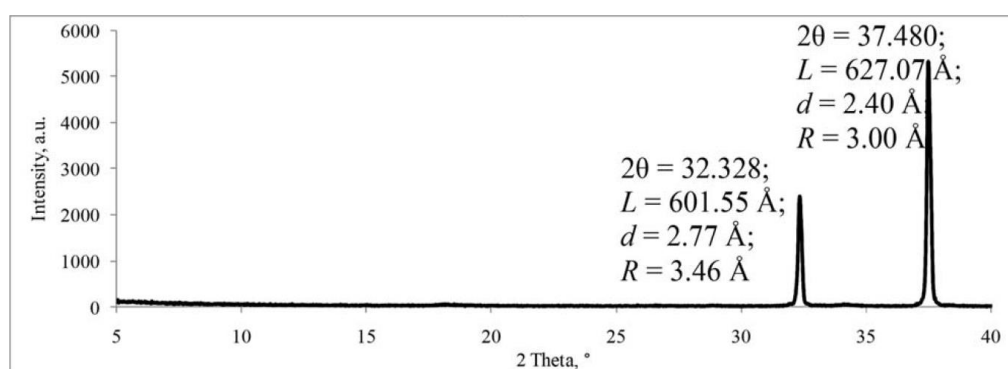
Figure 2.4 X-ray diffraction pattern of calcined eggshell powder at 2θ range of 5° to 40° (Bee *et al.*, 2017).

2.10   Characterization Analysis of Eggshell-PVOH Blends

2.10.1   Tensile Properties of Eggshell-PVOH Blends

The tensile strength of PVOH composites had increased gradually as the amount of CES added increased to 2 phr and obtained the greatest tensile strength of 57.6 MPa with 2 phr of CES by observing Figure 2.5a. This is because the CES enhanced of reinforcement effect of the PVOH matrix through interfacial adhesion and interaction between them. The reinforcement effect resulted in transferring stress subjected on the polymer composites through the particles to the polymer matrix effectively. Moreover, by adding CES, it could provided additional hydrogen bonds with the PVOH matrix (Bee *et al.*, 2017). Therefore, the tensile strength of the PVOH composites had increased because of the strong interaction between CES and PVOH.

However, when the amount of CES added was greater than 2 phr, the tensile strength of the PVOH composites was found decreased significantly. Agglomeration of CES particles occurred in PVOH composites due to the uneven dispersion of CES particles when greater amount of CES was added into the PVOH matrix. The agglomeration of CES particles in PVOH composites had led to ineffective in transferring the stress acted on PVOH matrix from the agglomerated CES particles by reducing the interfacial adhesion between the CES particles and PVOH (Bee *et al.*, 2017).

On the other hand, by referring to Figure 2.5b, pure PVOH was found to have the greatest elongation at break as compared to the CES-PVOH composites. This is because the non-restricted polymer chains of the pure PVOH were able to slip freely when it is subjected to the strain. In addition, from Figure 2.5b, the elongation at break of the PVOH composites was decreased gradually as the amount of CES added increased up to 2 phr and decrease when amount of CES added increased up to 5 phr. This is because of the presence of the effective interfacial adhesion between the CES particles and PVOH matrix had led to the restriction of mobility of the polymer chains of PVOH when subjected to straining stress. Furthermore, when the amount of CES added increased up to 5 phr, it had made the interfacial adhesion between the PVOH matrix and CES particles become weaker and led to uneven distribution of calcined eggshell particles. This had further promoted the formation of agglomeration of CES particles and impeded the flow of polymer chains when it was subjected to strain.
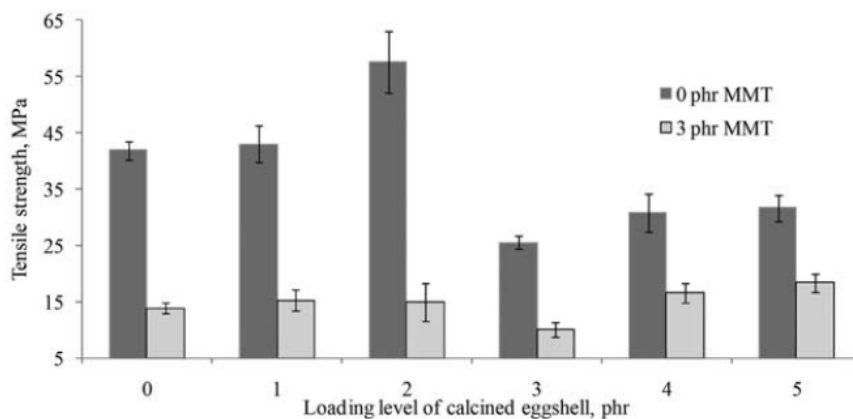
(a)
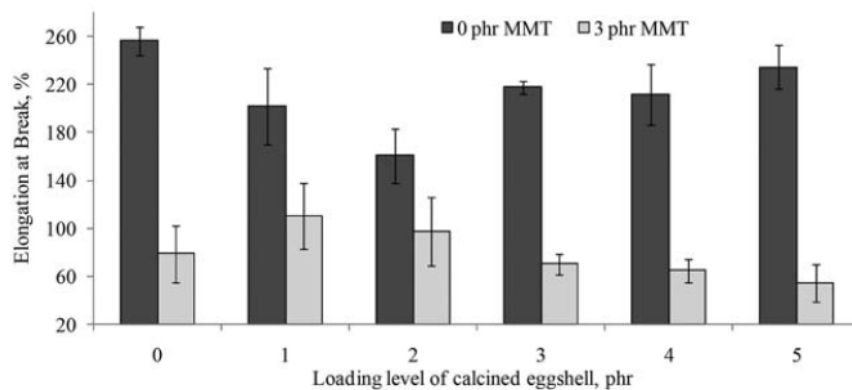
(b)

Figure 2.5 Effect of increasing of calcined eggshell loading level on (a) Tensile strength and (b) Elongation at break of PVOH and PVOH/MMT blends (Bee *et al.*, 2017)

2.10.2 SEM Analysis of Eggshell-PVOH Blends

By referring Figure 2.6, the agglomerated particles were able to be observed in the all of the PVOH composites added with CES while absence in the pristine PVOH. The occurrence of agglomeration of particles because the inhomogeneous dispersion of CES particles in the PVOH composites.

(a)   (b)

(c)   (d)
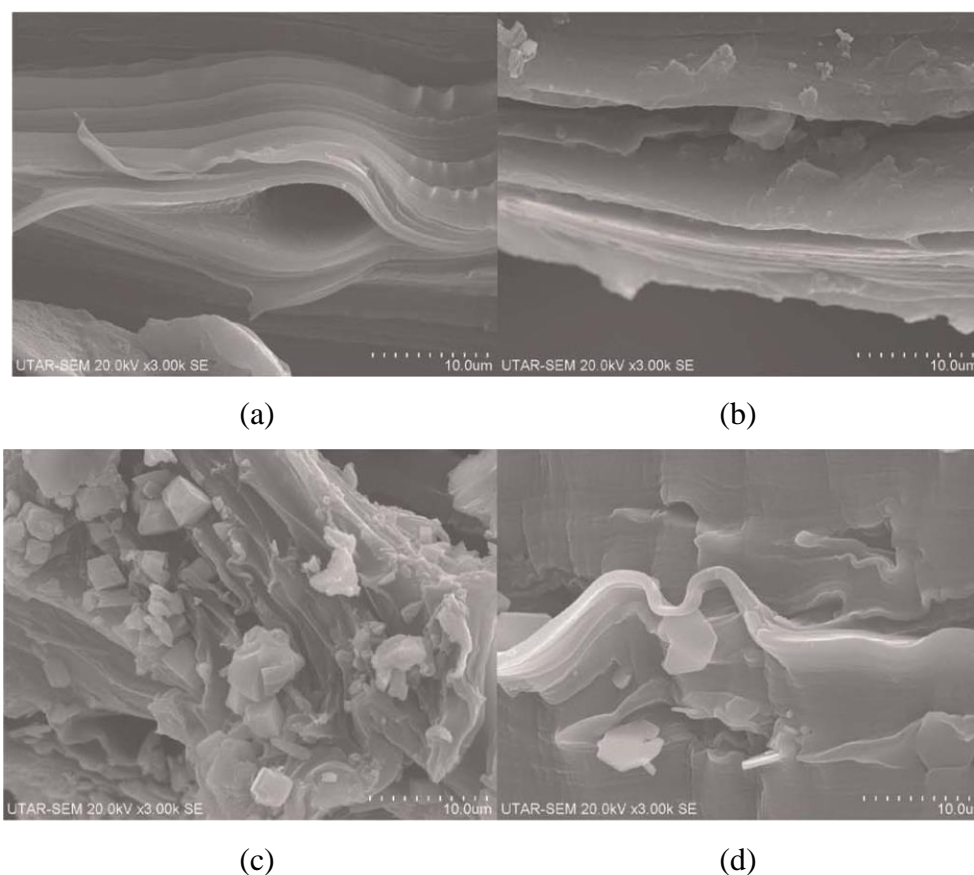
Figure 2.6 SEM morphologies of (a) pristine PVOH and PVOH added with (b) 1 phr (c) 3 phr and (d) 5 phr of calcined eggshell (Bee *et al.*, 2017).

2.10.3   XRD Analysis of Eggshell-PVOH Blends

Figure 2.7 had showed the XRD curves of the PVOH composites with increasing amount of CES. It had indicated that there were two significant deflection peaks occurred at 2θ range of 19° to 20° and 37° to 38° and they were known as the peak A and peak B respectively. The broad peak was indicating the existence of small crystallite size while sharp peak was indicating the existence of bigger crystallite size. Besides that, the humping effect had occurred on baseline of the XRD curve of the PVOH composites was observed due to the PVOH composites were partially crystallite with mainly amorphous phase (Bee *et al.*, 2017).

The deflection peak A was found sharpened significantly when amount of CES increased up to 3 phr from Figure 2.7. In addition, crystallite size of peak A was also found increased as the amount of CES added increased up to 3 phr based on Table 2.2. The crystallite size of the peak A could be induced by

interaction of small CES crystallites with regular crystallite peak A of the PVOH composites when a suitable amount of CES was added into it. However, when the amount of CES added further increased up to 5 phr, the crystallite size of the peak A had decreased gradually. When greater amount of CES was added, agglomeration of CES particles occurred. Therefore, the crystallite size of the peak A was decreased since agglomeration of CES could weaken the interaction between the crystallites of CES and originally existing peak A of PVOH composites.
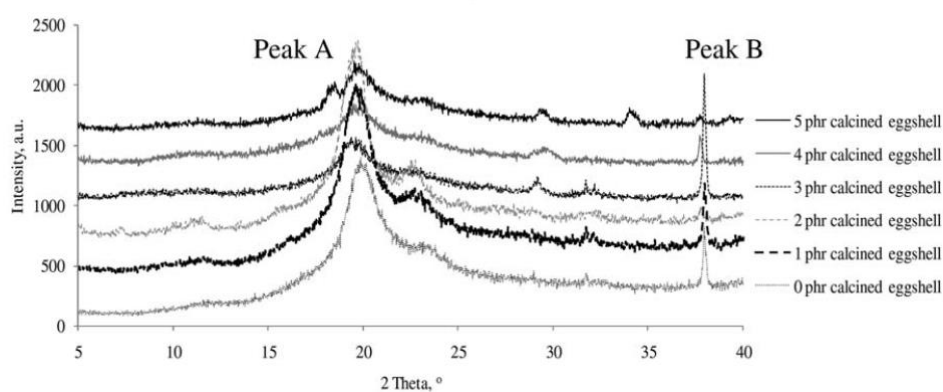
Figure 2.7 XRD curves of PVOH blends added with various loading levels of calcined eggshell at 2θ range of 5° to 40° (Bee *et al.*, 2017).

Table 2.2: Two Theta, crystallite size, *d*-spacing, and interchain separation of deflection peak A and B added with different loading levels of calcined eggshell (Bee *et al.*, 2017).

Loading level of calcined eggshell, phr	2 Theta (2θ), °	Crystallite size (L), Å	*d*-spacing, Å	Interchain separation (R), Å
Deflection peak A				
0	20.00	38.3	4.44	5.54
1	19.68	45.1	4.51	5.64
2	19.49	51.8	4.55	5.70
3	19.34	56.6	4.59	5.74
4	19.76	32.0	4.49	5.60
5	19.74	35.2	4.49	5.60
Deflection peak B				
0	37.94	151.8	2.37	2.97
1	37.93	148.2	2.37	2.97
2	37.73	136.3	2.38	2.98
3	37.94	539.6	2.37	2.97
4	37.73	162.1	2.38	2.98
5	37.74	150.7	2.38	2.98

By referring to Figure 2.7 and Table 2.2, the crystallite size of peak B was found to decrease as the deflection peak B of PVOH composites were broadened when the amount of CES added increased from 0 phr to 2 phr. This is because of the highly ordered chain structure of the crystallite of the peak B could broke when added low amount of CES into the PVOH composites. However, when the amount of CES added further increased to 3 phr, the crystallite size of the peak B had increased significantly due to the non-homogeneous dispersion and agglomeration of the CES particles. Furthermore, when the amount of the CES further increased to 5 phr, the crystallite size of the peak B had decreased significantly. Greater amount of CES added reduced the interaction between the crystallites and further broke the highly ordered crystallite structures of the peak B (Bee *et al.*, 2017).

2.10.4 FTIR Analysis of Eggshell-PVOH Blends

According to Figure 2.8 and Table 2.3, all PVOH composites added with various amount of CES had possessed a significant peak at the band range of 3200 cm^{-1} - 3600 cm^{-1}. It indicated the stretching of the hydroxyl group (O-H). The wavenumber of O-H stretching band was found slightly shifted to left and

resulted in greater wavenumber as the amount of CES added increased to 5 phr. The addition of CES induced the interaction between CES particles and the polymer chains of PVOH and further slightly reduced the strength of the hydrogen bonding. However, there was a slightly drop of wavenumber of hydroxyl band when amount of CES added further increased to 3 phr. This is because the agglomeration of CES particles occurred in the PVOH composites and it could induce the hydrogen bonds.

In addition, at region with wavenumber of 2900 cm^{-1}, a peak which indicating the appearance of the stretching of C-H bond was observed when the amount of CES added increased up to 3 phr. However, the peak was found disappeared when the amount of CES added increased from 3 phr to 5 phr. According to Bee *et al.* (2017), this is because of the formation of the intermolecular complexes had caused the intermolecular vibrations to be affected.

The occurrence of bending of O-H bond was observed at the wavenumber of 1328 cm^{-1} in the FTIR spectrum of the PVOH composites with 0 phr of CES and the peak of O-H bending was found to disappear as the amount of CES added increased. This is because of the presence of strong interaction effect between hydroxyl group (O-H) and CES particles (CaO) which would hinder the O-H bending in the PVOH composites.
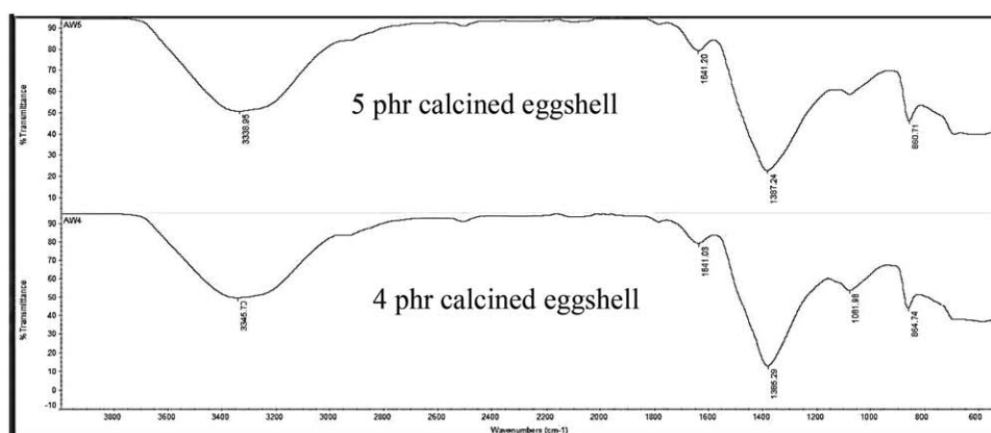
(a)
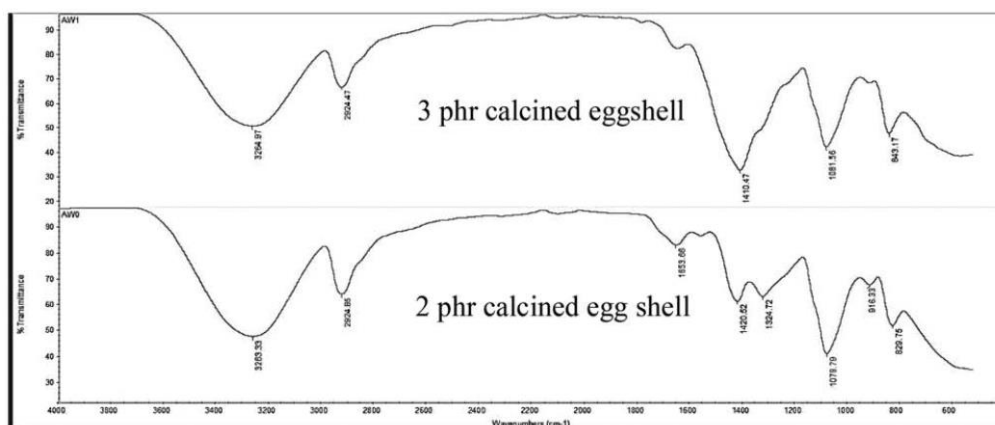
(b)
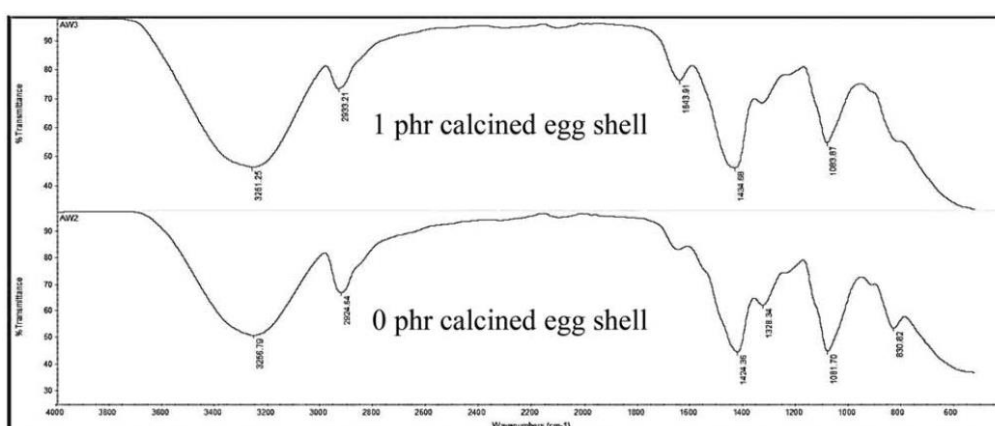
(c)

Figure 2.8 FTIR Spectrum of PVOH blends added with various loading levels of calcined eggshell (a) 5 phr and 4 phr, (b) 3 phr and 2 phr, and (c) 1 phr and 0 phr (Bee *et al.*, 2017).

Table 2.3: Wavenumber of hydroxyl group (-OH) and C-H stretching of PVOH blends added with calcined eggshell (Bee *et al.*, 2017).

Loading level of calcined eggshell, phr	-OH bonding wavenumber, cm^{-1}	C-H stretching wavenumber, cm^{-1}
0	3263.33	2924.85
1	3264.97	2924.47
2	3265.79	2924.64
3	3261.25	2933.21
4	3345.70	-
5	3338.95	-

2.11   Water Absorption Test for PVOH-HAp Composite Hydrogel

From the research conducted by Azzaoui *et al.* (2014), the water absorption of the HAp composites increased when reducing the HAp composition. The statement was supported by the Figure 2.12, the 10/80/10 composite had the lowest swelling ratio of 51%.
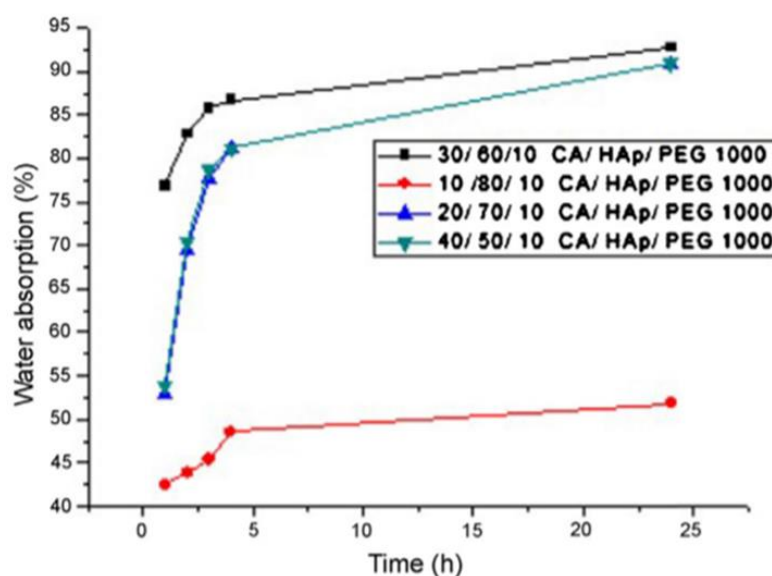
Figure 2.9 Swelling ratio of cellulose acetate-hydroxyapatite-polyethylene glycol (CA/HAp/PEG) composite (Azzaoui *et al.*, 2014).

2.12   Summary

The general background of the materials and analysis methods used in this study were being covered in this chapter. Furthermore, the characterization analysis results from other researchers which could become the guidelines in this study.

CHAPTER 3

METHODOLOGY AND WORK PLAN

3.1 Materials

Fully hydrolysed PVOH manufactured by Denki Kagaku Kougyo Kabushiki Kaisya (DENKI) with grade of Denka Poval, K-17C was used as the polymer base in this study. The hydrolysis and viscosity of the PVOH were 87 mol% to 89 mol% and 45 mPa.s to 55 mPa.s respectively. Besides that, the green mussel shells were collected from Seremban district in Negeri Sembilan state.

3.2 Formulation

There were 6 samples prepared with different loading level of hydroxyapatite in this study as shown in Table 3.1. The amount of PVOH used in casting was fixed at 100 phr with different amount of hydroxyapatite. Table 3.1 had showed the abbreviation of samples.

PH - _

Table 3.1: Abbreviation of samples.

Letter	Stands for
P	PVOH
H	HAp
Third letter	Amount of HAp in phr

Table 3.2: Formulation of mussel shell-PVOH blends.

Sample	PVOH (phr)	HAp (phr)
PH-0	100	0
PH-1	100	1
PH-2	100	2
PH-3	100	3
PH-4	100	4
PH-5	100	5

3.3 Sample Preparation

The green mussel shells were collected and cleaned thoroughly with tap water to get rid of the impurities. The shells were boiled in boiling water for 1 hour and cleaned with brush to further remove any organic matter attached on it.

After the cleaning steps, the green mussel shells were dried and crushed into smaller pieces. After that, the shells were calcined under 900 ℃ with furnace for two hours. The calcined mussel shells were later grinded into fine powder with the porcelain mortar.

Mussel shell-PVOH composite samples were prepared by using solution casting method. Initially, the PVOH resin was dissolved in distilled water and heated by a water bath of 97℃ ± 2℃ for 30 minutes. The mixture was agitated at speed of 350 rpm with magnetic stirrer until all the PVOH resin dissolved completely in the distilled water. After that, the calcined mussel shell powder was added into the PVOH solution and the mixture continued agitated and heated until all the calcined mussel shell powder was dissolved completely. Then, the PVOH mixture was casted into a film by pouring it into a petri dish with thickness of approximately 1mm. After that, the film was dried in the oven at temperature of 50℃ for 2 days. The remaining formulation samples in Table 3.1 were prepared by repeating the same steps. The dried samples were kept in the sealed plastic bag and stored under room temperature of 25℃.

3.4   Characterization Test for PVOH-HAp Composites

3.4.1   Tensile Test

Tensile test was carried out with Tinius Olsen H10KS Tensile Microtester in accordance to ASTM D882. The samples were cut into a rectangular shape with 60 mm in length and 6 mm in width. The dimensions of specimen were measured using Vernier scale before the tensile testing. The specimen was pulled with a straining rate of 50 mm/min and cell load of 5 kN. The tensile strength, Young's modulus and elongation at break of the sample were measured and recorded. 5 specimens for each formulation were tested to get the average value.

3.4.2   Scanning Electron Microscopy (SEM)

The surface morphologies of the specimens were observed using a Hitachi S3400N SEM machine. The fractured surfaces of samples were cut into small portion before mounted onto the specimen stub with fractured surface facing

upwards. A layer of gold and palladium was used to cover the mounted samples with the use of EMITECH SC7620 Sputter Coater. The samples were scanned and the SEM micrographs were observed and recorded at the magnification of 300 times, 800 times and 1000 times.

3.4.3   X-ray Diffraction (XRD)

A Shimadzu XRD 6000 X-ray Diffractometer (XRD) was used to determine the crystallinity and crystallography structures of the samples. The X-ray spectra was recorded with diffractometer using Cu-Kα radiation with wavelength of 1.542 Å produced by a Cu-Kα generator operated at 30 mA of current and 40 kV of acceleration voltage. The samples were scanned at rate of 1.2 °/min with scattering angles (2θ) range from 5° to 40°. The d was determined by using Bragg's equation as shown in equation 5. Besides, the R was calculated using Klug and Alexander equation as shown in equation 6 and the L was determined using Scherrer equation as shown in equation 7.

$$d = \frac{\lambda}{2 \sin \theta} \tag{5}$$

$$R = \frac{5\lambda}{8 \sin \theta} \tag{6}$$

$$L = \frac{K\lambda}{\beta \cos \theta} \tag{7}$$

Where λ is 1.542 Å,

θ is Bragg angle in radians,

K is the Scherrer constant,

β is the full width at half maximum of deflection peak.

3.4.4   Water Absorption Test

Water absorption test was carried out by immersing the samples into distilled water for 1 day. Before immerse into distilled water, the samples were cut into 5 pieces of specimens with same size and the initial weight (W_i) of each specimen was weighted and recorded. The specimens were weighted again to obtain final weight (W_f) after 1 day. The water absorption test was kept repeating until the percentage of water uptake become constant. The percentage of water uptake (M_t) can be determined by applying the equation below:

$$M_t = \frac{W_f - W_i}{W_i} \times 100\% \qquad (8)$$

3.4.5   Fourier Transform Infrared Spectroscopy (FTIR)

Fourier transform infrared analysis was performed using Nicolet IS10-FTIR Spectrometer to determine the presence of specific chemical groups in the samples. The samples were placed at the centre of the diamond crystal in the centre of ATR plate. The press of ATR was lowered and the samples were scanned under spectrum range from 4000 cm^{-1} to 400 cm^{-1}.

3.5   Summary

In this chapter, it had covered the methods to prepare the calcined mussel shell and sample, formulation for each samples and the methods to undergo the characterization test.

CHAPTER 4

RESULTS AND DISCUSSION

4.1   Characterization Test for Calcined Mussel Shell

4.1.1   Scanning Electron Microscopy of Calcined Mussel Shell

Figure 4.1 shows the SEM micrograph of the calcined mussel shell powder at the magnification of 5000X. The surface morphologies of the calcined mussel shell can be observed by using the SEM. From Figure 4.1, the particles of calcined mussel shell powder are in irregular shape and tended to pack together. Besides that, the calcined mussel shell particles had particle size range from approximately 3 µm to 8 µm.
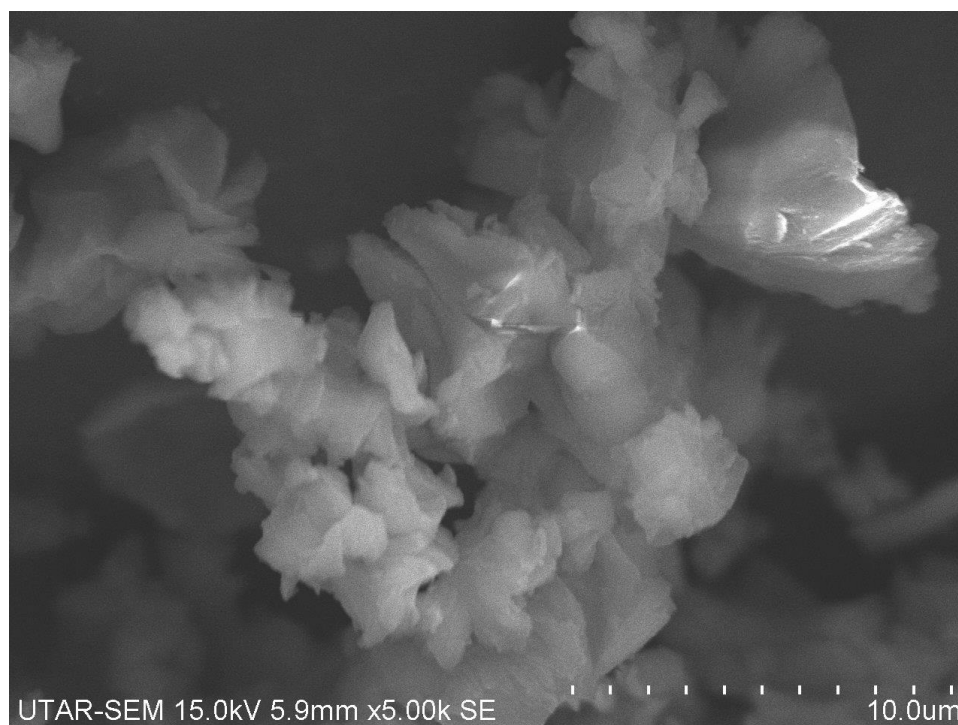
Figure 4.1 SEM micrograph of calcined mussel shell powder at magnification of 5000X.

4.1.2   Energy Spectra X-ray Analysis of Calcined Mussel Shell

Figure 4.2 shows the result of EDX analysis for the calcined mussel shell powder. From Figure 4.2, the main compositions of calcined mussel shell

powder were composed of two elements, which are calcium and oxygen. The weight percentage and atomic percentage of oxygen and calcium are showed in the Table 4.1. The result obtained has proven that the main composition of mussel shell is calcium carbonate ($CaCO_3$) and it oxidized to form calcium oxide (CaO) and carbon dioxide (CO_2) during calcination process. The chemical reaction is showed in the equation 9.

$$CaCO_3 \rightarrow CaO + CO_2 \tag{9}$$
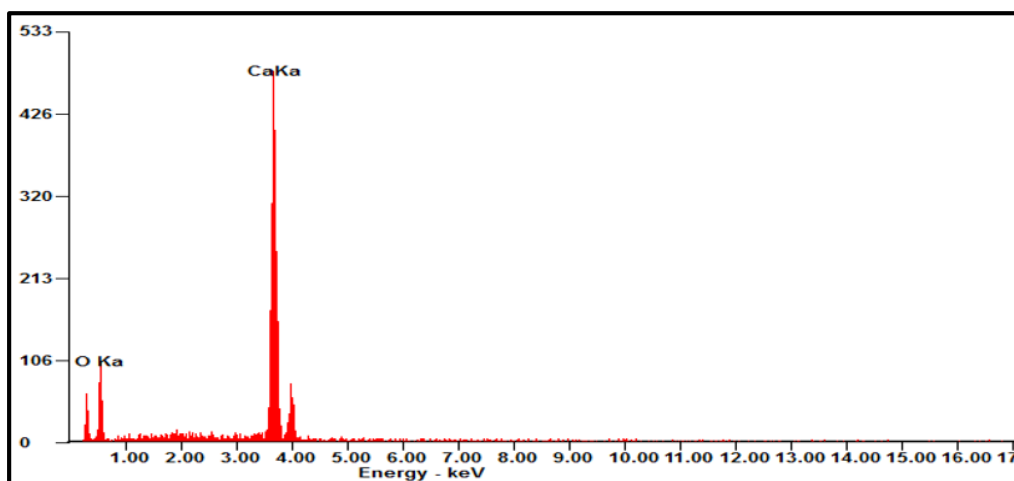
Figure 4.2 Energy Spectra X-Ray analysis result of calcined mussel shell.

Table 4.1: Composition of calcined mussel shell in weight percentage and atomic percentage.

Element	Wt%	At%
O	39.92	62.47
Ca	60.08	37.53

4.1.3 X-ray Diffraction Analysis of Calcined Mussel Shell

By referring to Figure 4.3, there are several peaks can be observed in the XRD curve of pure calcined mussel shell. For instance, the peaks are located at 2θ of 18°, 29°, 34° and 37°.
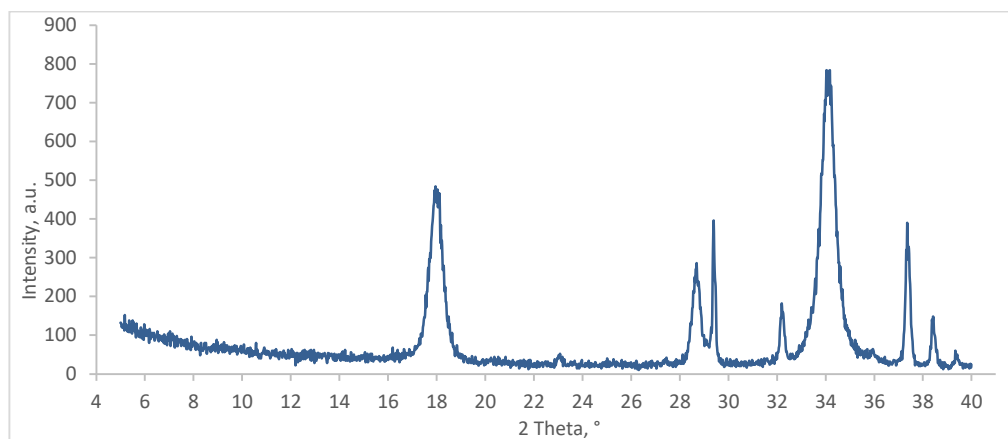
Figure 4.3 XRD curve of calcined mussel shell at 2θ range of 5° to 40°.

4.2 Characterization Test for PVOH/Calcined Mussel Shell Composites

4.2.1 Tensile Test for PVOH/Calcined Mussel Shell Composites

4.2.1.1 Tensile Strength

According to Figure 4.4, the tensile strength of the PVOH increased slightly when added with 1 phr of calcined mussel shell and increased significantly when increased to 2 phr. The tensile strength of PVOH/calcined mussel shell composites reached the highest value of 35.49 MPa when added with 2 phr of calcined mussel shell powder. This might due to the presence of interfacial adhesion and also the interaction between the PVOH matrix and calcined mussel shell particles, where the small amount of calcined mussel shell (≤ 2 phr) could provide good dispersion and further enhanced the hydrogen bond that formed by the O-H functional group of the PVOH matrix. Good dispersion of calcined mussel shell particles also provided reinforcement to the PVOH matrix and resulted in greater tensile strength (Bee *et al.*, 2017).

And yet, the tensile strength of the PVOH/calcined mussel shell composites decreased gradually when calcined mussel shell further increased up to 4 phr. This is because of the improper dispersion of calcined mussel shell in PVOH occurred which leads to the agglomeration of the calcined mussel shell particles. The agglomerate particles could weaken the tensile strength of the PVOH/calcined mussel shell composites by reducing bonding interaction

between the calcined mussel shell and PVOH. Moreover, the agglomerate particles also acted as the stress concentration point during straining where the stress unable to be transferred to the PVOH matrix effectively.
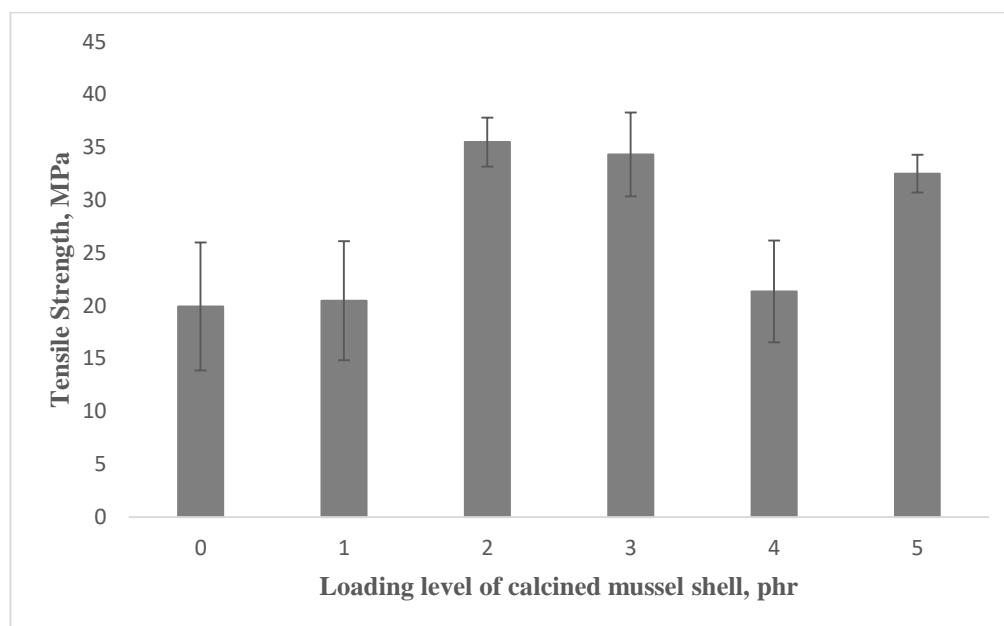
Figure 4.4 Tensile strength of PVOH composites with different loading level of calcined mussel shell.

4.2.1.2 Young's Modulus

Figure 4.5 shows the Young's modulus of the PVOH/calcined mussel shell composites when different amount of calcined mussel shell was added. The Young's modulus of the PVOH composites went through a significant increment of 219 % when amount of calcined mussel shell added increased to 2 phr. This is due to the addition of calcined mussel shell could induce the formation of hydrogen bonding and interfacial adhesion between the PVOH matrix and calcined mussel shell particles. Furthermore, the calcined mussel shell could act as a reinforcing agent within the PVOH matrix and increased the rigidity of the PVOH composites. Therefore, the Young's modulus increased as the rigidity of PVOH composites increased.

As the amount of the calcined mussel shell further increased to 5 phr, the Young's modulus of PVOH composites started to show a decrement trend. Greater amount of calcined mussel shell ($\geq$ 3 phr) caused the poor dispersion of calcined mussel shell particles and formed agglomerate. The agglomeration of

calcined mussel shell particles weakened the interfacial adhesion between calcined mussel shell particles and PVOH matrix, further lower the rigidity of the PVOH composites. Thus, the Young's modulus decreases with the rigidity of PVOH composites.
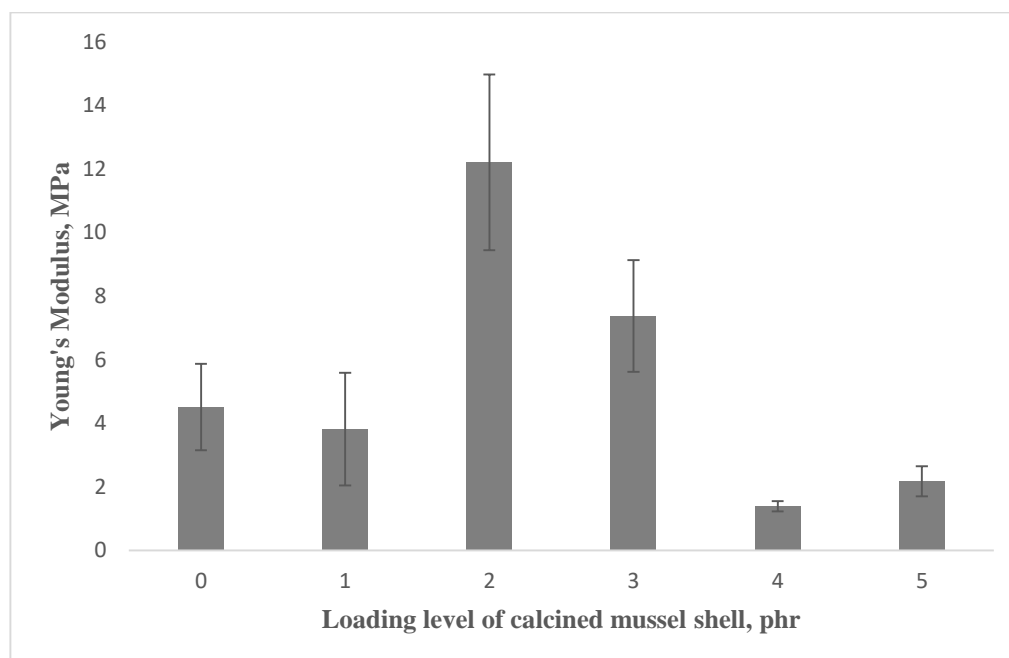
Figure 4.5 Young's modulus of PVOH composites with different loading level of calcined mussel shell.

4.2.1.3 Elongation at Break

By referring to Figure 4.6, the elongation at break of the pure PVOH was found to be the lowest value of 144.5 % while the elongation at break of the PVOH composites increased gradually when amount of calcined mussel shell increased up to 3 phr. This might due to the lower loading level of calcined mussel shell able to provide reinforcement effect by introducing better interaction between the calcined mussel shell and PVOH. Consequently, the chain mobility of the PVOH composites increased due to the better interaction and enhanced the elongation at break.

Conversely, the elongation at break of the PVOH composites decreased from 242.03 % to 206.67 % when the amount of the calcined mussel shell increased from 3 phr to 4 phr. This is because of the formation of agglomerated

calcined mussel shell tends to prevent the chain to slide against each other, thus reduced the mobility of polymer chain in PVOH composites (Bee *et al.*, 2017).
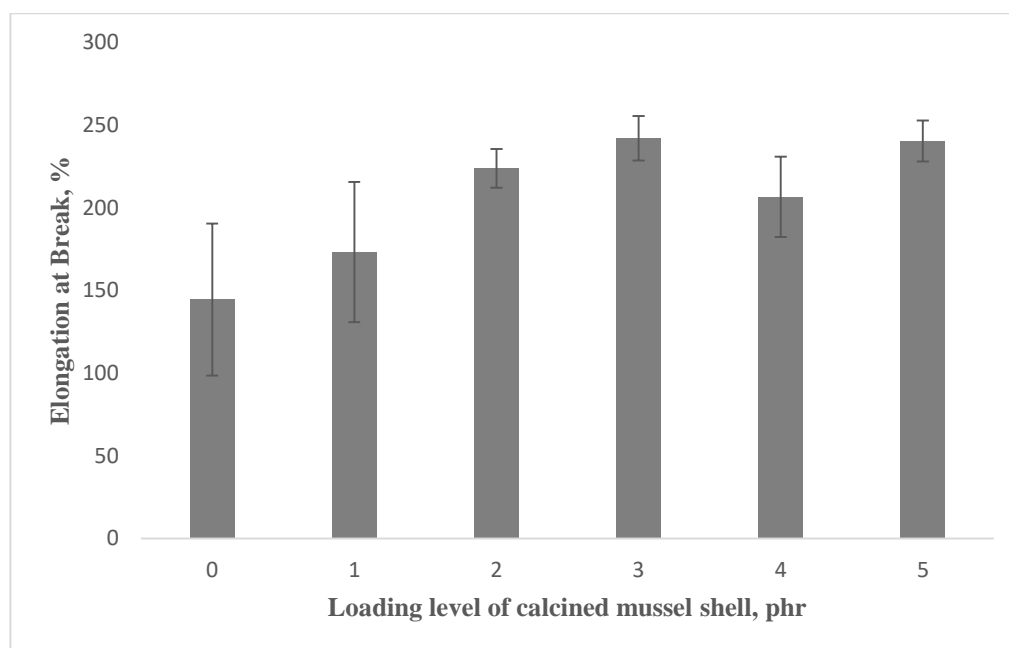
Figure 4.6 Elongation at break of PVOH composites with different loading level of calcined mussel shell.

4.2.2 Scanning Electron Microscopy (SEM) for PVOH/Calcined Mussel Shell Composites

By referring to Figure 4.7, the surface morphologies of the PVOH/calcined mussel shell composites were observed by SEM. There are few traits can be found in the morphologies of fractured surface of PVOH composites. For instance, cavities, fibril, tearing effect, wave like structure, matrix continuity, flake like structure and agglomerated particles.

By observing Figure 4.7, there were void or holes which also known as cavities can be found in the PVOH matrix of pure PVOH and PVOH composite added with 1 phr of calcined mussel shell but did not appear in PVOH composites with greater amount of calcined mussel shell ($\geq$ 2 phr). This indicating the calcined mussel shell particles could diminish the occurrence of cavities in the PVOH matrix. The cavities could turn into weak point of the PVOH composites, when it is subjected to straining, the cavities will become the stress concentration point and it will be torn apart from there. Therefore, the

cavities in PVOH composites could lead to low tensile strength and low Young's modulus.

On the other hand, the flake like structure can be observed in the PVOH composites with greater amount of calcined mussel shell as showed in Figure 4.7 (e) and (f). The occurrence of flake like structure is due to the non-homogenous dispersion of calcined mussel shell particles in the PVOH matrix, it weakens the interfacial adhesion effect and the interaction with PVOH matrix. Thus, the flake like structure of the calcined mussel shell particles acted as lubricant in the PVOH matrix when the PVOH composite undergo elastic deformation as it was subjected to straining. As a result, the flake like structure in PVOH composites will results in lower Young's modulus.

According to Figure 4.7 (c), high matrix continuity and wave like structure were found in the fracture surface of PVOH composite with 2 phr calcined mussel shell. Occurrence of high matrix continuity of polymer is because of the homogenous dispersion of calcined mussel shell particles provided stronger interfacial adhesion effect and also interaction between the PVOH matrix. Besides that, high matrix continuity also indicates lesser tearing effect and the weak point present in the PVOH matrix. Therefore, it leads to higher tensile strength. When the PVOH composite breaks during stretching, the wave like structure is formed due to the rebounding effect of elongated PVOH matrix. The wave like structure indicates the polymer has greater elongation under plastic deformation when subjected to straining.

Tearing effect could to be observed in Figure 4.7 (b), (c) and (d). Although the addition of calcined mussel shell into PVOH could induce interfacial adhesion effect and interaction with the polymer matrix, however poor dispersion of calcined mussel shell particles could weaken the effects. Thus, poor dispersion of calcined mussel shell particles increases the weak point or stress concentration point. This will cause the PVOH composites to break at the stress concentration point and lower the tensile strength.

By referring Figure 4.7 (b) and (c), the fibrils can be found at the fractured surface of the PVOH composites. The formation of fibrils is due to the elongation of PVOH matrix when subjected to straining. However, the PVOH composite with 3 phr calcined mussel shell had lesser amount of fibrils and the

fibrils were longer in length and thicker in width. This indicates it has stronger interaction between the PVOH matrix and calcined mussel shell particles and therefore greater tensile strength.
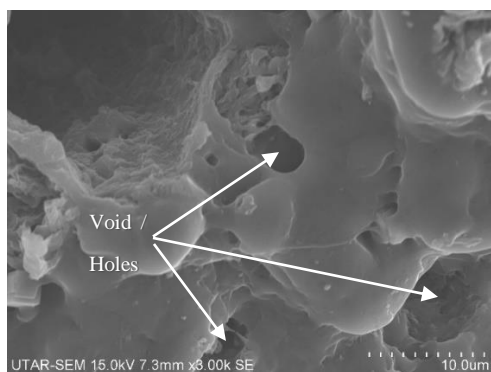
(a) Pure PVOH
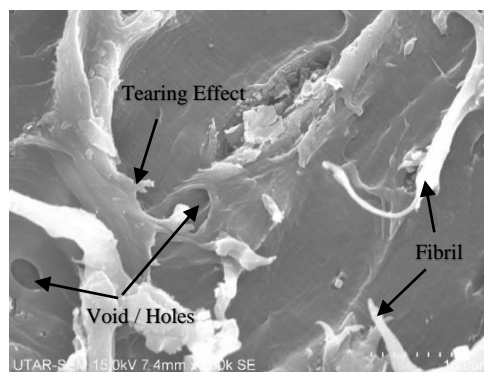
(b) 1 phr calcined mussel shell
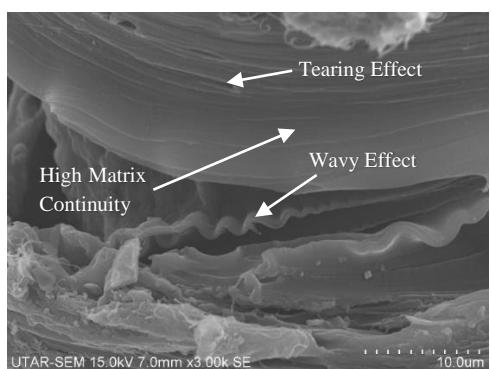
(c) 2 phr calcined mussel shell
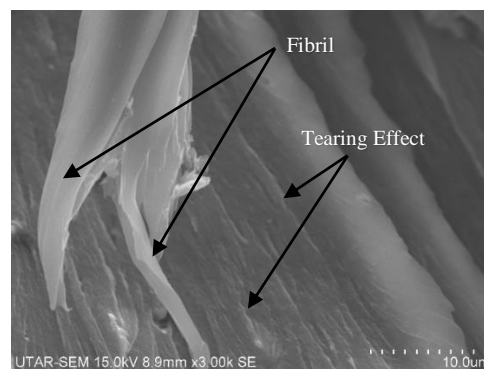
(d) 3 phr calcined mussel shell
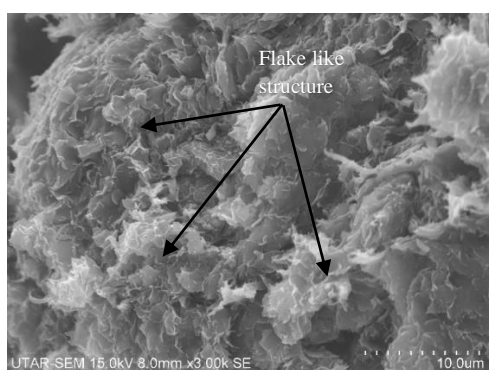
(e) 4 phr calcined mussel shell
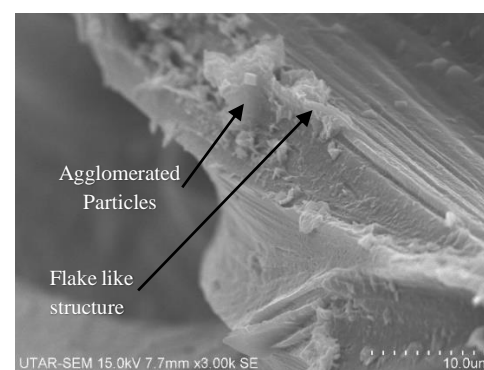
(f) 5 phr calcined mussel shell

Figure 4.7 Scanning Electron Microscopy of PVOH composites with different loading level of calcined mussel shell at magnification of 3000X.

4.2.3 X-ray Diffraction (XRD) Test for PVOH/Calcined Mussel Shell Composites

According to Figure 4.8, there are two peaks which are labelled as Peak C and Peak P occurred at 2 Theta (2θ) of 19° and 29° respectively in the XRD curves of PVOH/calcined mussel shell composites. Besides that, the humping effect was found to presence on the baseline of the XRD curves which indicating the PVOH composites are partially crystallite with dominant amorphous phase (Kumar *et al.*, 2012). The values of 2θ and FWHM of the deflection peaks were used to calculate the crystallite size, *d*-spacing and interchain separation and the results are listed in Table 4.2.

From Table 4.2, the crystallite size of Peak C decreased gradually from 48.97 Å to 47.75 Å when the amount of calcined mussel shell increased from 0 to 2 phr. This indicates the addition of small amount of calcined mussel shell could interrupt the arrangement of crystallite structure of PVOH matrix. However, the crystallite size increased as the amount of calcined mussel shell increased up to 5 phr and reached maximum value of 51.67 Å at 4 phr. This is because of the non-homogenous dispersion of the calcined mussel shell in the PVOH and the presence of agglomerated calcined mussel shell particles (Bee *et al.*, 2017).

By referring to Figure 4.8, Peak P did not appear in the XRD curves of PVOH composites with 0 phr and 1 phr of calcined mussel shell. However, when the loading level of calcined mussel shell increases, Peak P had occurred at 2θ of 29° to 30°. Besides, as compare with the XRD curve of calcined mussel shell in Figure 4.3, similar peak can be found at same 2θ, therefore, the addition of calcined mussel shell could induce the occurrence of Peak P. The crystallite size of Peak P decreased slightly when amount of calcined mussel shell increased from 2 to 3 phr and increased significantly when amount of calcined mussel shell increased up to 5 phr. This is because poor dispersion of calcined mussel shell has led to the formation of agglomerated particles and the agglomerated particles become bigger as the amount of calcined mussel shell increases.

Furthermore, the *d* and *R* for both of the Peak C and P are found to be less affected by the addition of calcined mussel shell which indicates the

presence of calcined mussel shell has less effect on the compactness of PVOH matrix.

There are two peaks occurred in the XRD curves of PVOH composites with 4 phr and 5 phr of calcined mussel shell at 2θ of 18° and 34° respectively. Both of the peaks only occurred when high loading level of calcined mussel shell ($\geq$ 4 phr) are added into PVOH composites. On the other hand, both of the peaks also can be found in the XRD curve of calcined mussel shell in Figure 4.3. Therefore, high loading level of calcined mussel shell in PVOH composites tends to agglomerate into larger particles and induces the peaks at 2θ of 18° and 34°.

According to Table 4.3, the crystallinity of PVOH composites increased from 9.89 % to 11.43 % when the amount of calcined mussel shell increased from 0 phr to 2 phr. The increment of crystallinity indicates the addition of calcined mussel shell has interrupt the ordered crystallite structure arrangement in PVOH matrix. However, the crystallinity decreased when amount of calcined mussel shell increased from 2 to 3 phr. This might because of the agglomeration of calcined mussel shell start to occur, hence weakened the interaction effect on the PVOH matrix. Besides that, the crystallinity has increased significantly as the loading level further increase up to 5 phr. The high crystallinity percentage might be contributed by the highly agglomerated calcined mussel shell particles present in the PVOH matrix.
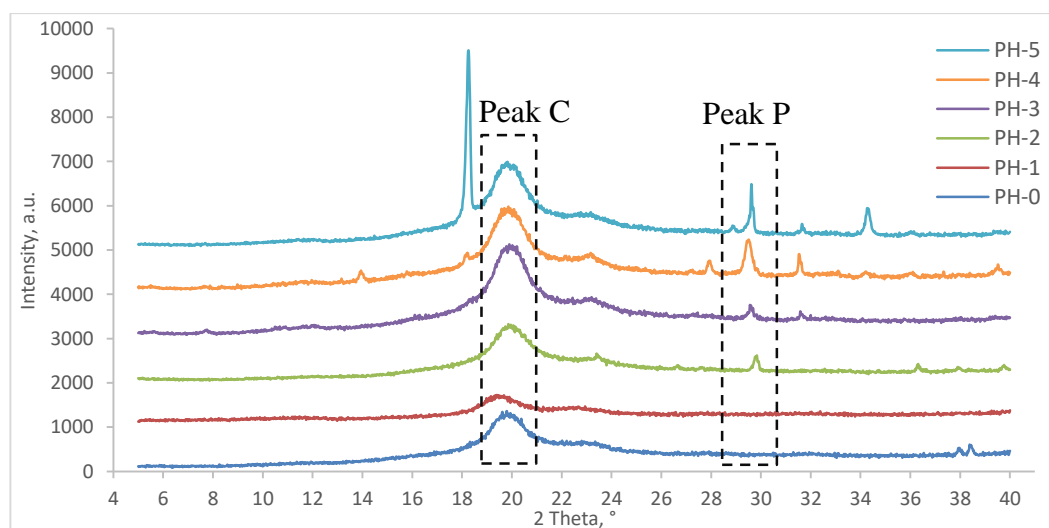
Figure 4.8 XRD curves of PVOH composites with different loading level of calcined mussel shell at 2θ range of 5° to 40°.

Table 4.2: Crystallite size, *d*-spacing, and interchain separation of deflection peak C and P of PVOH composites with different loading level of calcined mussel shell.

Calcined Mussel Shell Loading Level, phr	2 Theta (2θ), °	*d*-spacing (d), Å	Interchain Separation (R), Å	Crystallite Size (L), Å
Peak C				
0	19.8452	4.4679	5.5849	48.9699
1	19.5621	4.5319	5.6649	48.5216
2	19.9798	4.4381	5.5477	47.7496
3	19.9250	4.4502	5.5628	50.8990
4	19.8667	4.4631	5.5789	51.6680
5	19.7800	4.4825	5.6031	50.5479
Peak P				
0	-	-	-	-
1	-	-	-	-
2	29.7639	2.9977	3.7472	167.6029
3	29.5621	3.0177	3.7722	157.0598
4	29.4723	3.0267	3.7834	158.9865
5	29.6090	3.0131	3.7663	561.7421

Table 4.3: Crystallinity of PVOH composites with different loading level of calcined mussel shell.

Calcined Mussel Shell Loading Level, phr	Crystallinity, %
0	9.89
1	10.16
2	11.43
3	9.87
4	12.12
5	14.84

4.2.4 Water Absorption Test for PVOH/Calcined Mussel Shell Composites

According to the Figure 4.9, the pristine PVOH tends to have the greatest capability to absorb more water whereas the PVOH composite added with 2 phr of calcined mussel shell has the lowest capability to absorb water. This is because of the pristine PVOH is more hydrophilic due to the absent of calcined mussel shell particles inside it, thus it can form more hydrogen bond with the water molecules and results as higher water absorption capability (Gilormini and Verdu, 2018). Moreover, the PVOH composite with 1 phr of calcined

mussel shell also has higher water absorption capability than other PVOH composites since it has similar properties with the pristine PVOH.

On the other hand, the PVOH composite added with 2 phr of calcined mussel shell has better dispersion of calcined mussel shell particles that enhanced the interaction with the PVOH matrix and more calcined mussel shell particles able to form hydrogen bond with the PVOH matrix. Therefore, less water molecules are able to form hydrogen bond with the PVOH matrix.

Besides that, the formation of agglomerated calcined mussel shell particles also enhanced the water absorption capability of PVOH composites slightly. By referring to the Figure 4.9, the PVOH composites with greater amount of calcined mussel shell ($\geq$ 3 phr) has lower water absorption capability than pristine PVOH and slightly higher water absorption capability than the PVOH composite added with 2 phr calcined mussel shell. Agglomeration of calcined mussel shell particles tends to occur at higher loading level and it had been proven in the scanning electron microscopy (SEM). Agglomerated calcined mussel shell particles reduced the strength of hydrogen bond with PVOH matrix so that the water molecules could form hydrogen bond with the PVOH composites.

The overall trend of the results of water absorption test showed that all of the samples were saturated with water after immersed in distilled water for 8 hours. There are only little changes in the weight of every samples after immersed in distilled water for 8 hours.
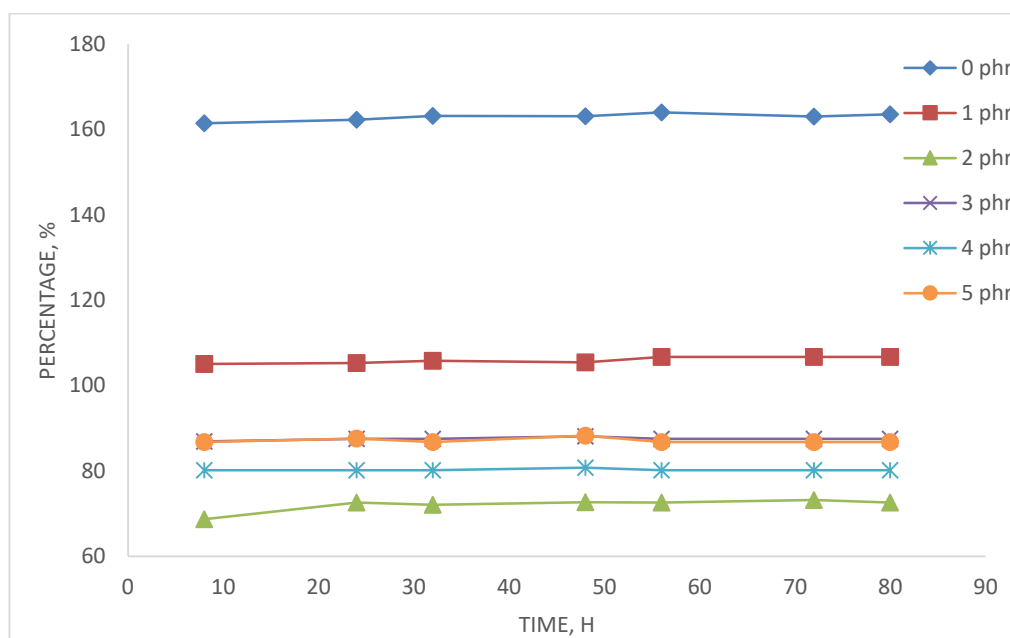
Figure 4.9 Changes in weight of PVOH composites with different loading level of calcined mussel shell.

Table 4.4: Average water absorption capability of PVOH composites with different loading level of calcined mussel shell.

Calcined Mussel Shell Loading Level, phr	Average Percentage, %	Standard Deviation
0	162.95	0.8487
1	106.00	0.7418
2	72.07	1.5207
3	87.53	0.3501
4	80.26	0.2210
5	87.10	0.6198

4.2.5 Fourier Transform Infrared Spectroscopy (FTIR) for PVOH/Calcined Mussel Shell Composites

Figure 4.10 shows the FTIR spectrum of PVOH/calcined mussel shell composites with different amount of calcined mussel shell. From Figure 4.10, a significant peak can be observed at the band of 3254 cm^{-1} to 3335 cm^{-1} for all samples, which indicating the occurrence of O-H stretching of the hydroxyl group (O-H). According to the Figure 4.10 and Table 4.5, the wavenumber of the O-H stretching band decreased gradually from 3268.41 cm^{-1} to 3254.01 cm^{-1} as the amount of the calcined mussel shell increased from 0 phr to 2 phr. The decrement of the wavenumber of the O-H stretching band indicates the

hydrogen bonding in the PVOH composites has increased. Good dispersion of the calcined mussel shell able to enhance the interaction between calcined mussel shell and PVOH and further induces the hydrogen bonding. However, the peak of O-H stretching band shifted to left when the calcined mussel shell further increased to 5 phr. This is because of the agglomeration of calcined mussel shell occurred and lead to poor interaction. The agglomerated calcined mussel shell particles reduced the strength of hydrogen bonding within the PVOH (Bee *et al.*, 2017).

On the other hand, by referring to Figure 4.10, the peak of C-H stretching was found at the wavenumber of around 2940 cm^{-1}. The wavenumber of C-H stretching remained almost constant at 2939 cm^{-1} when the amount of calcined mussel shell increased up to 2 phr. This situation indicates the addition of low loading level of calcined mussel shell did not bring big impact to the C-H bonding of the PVOH matrix. However, the wavenumber decreased significantly as the calcined mussel shell increased from 2 to 3 phr. This is because of the addition of calcined mussel shell able to interact with the PVOH matrix and form new hydrogen bond. Thus, the C-H bonding was weakened by the formation of new hydrogen bond. When the amount of calcined mussel shell further increased to 5 phr, the peak of C-H stretching shifted to left and results in increment of wavenumber. Agglomeration of calcined mussel shell particles occurred at high loading level and result in weakening of hydrogen bond, so the strength of C-H bonding was enhanced with the occurrence of agglomeration of calcined mussel shell particles.
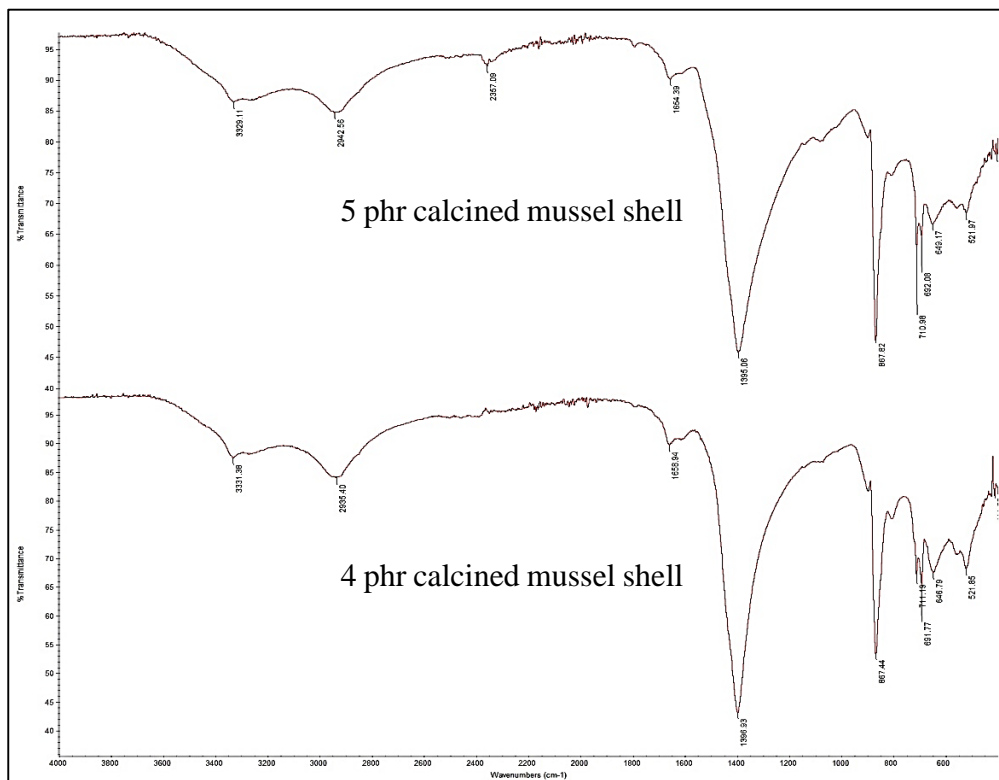
(a)
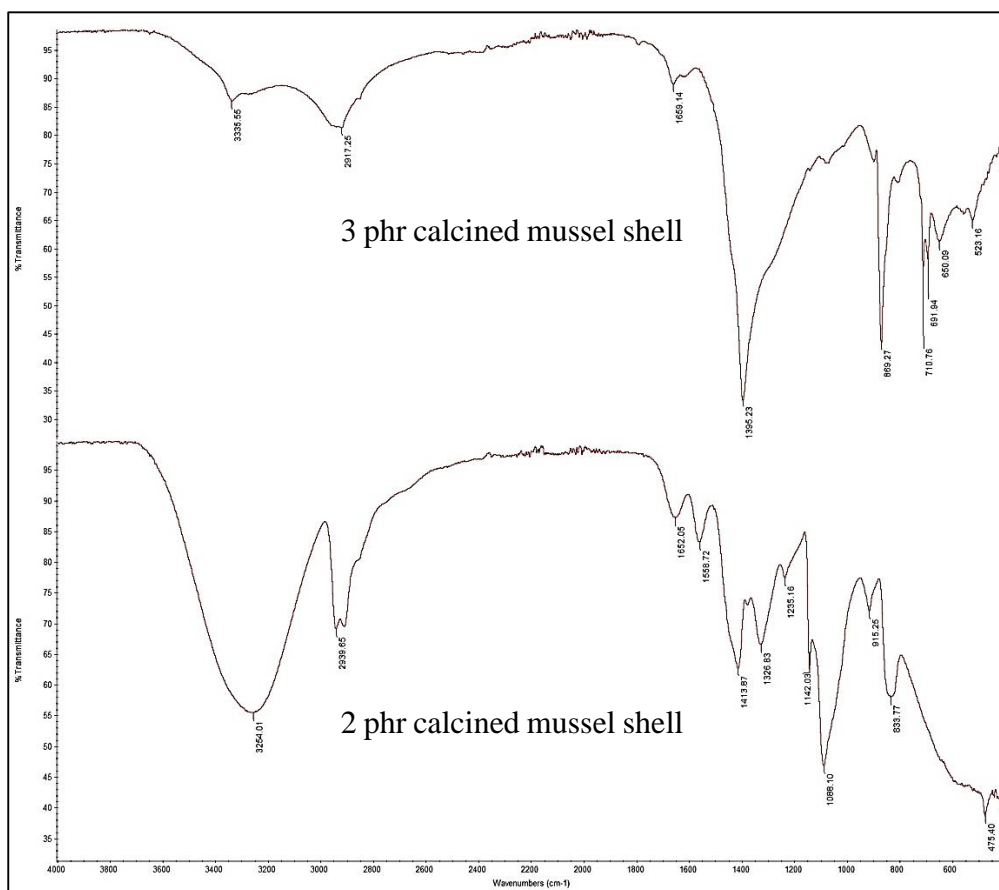
(b)
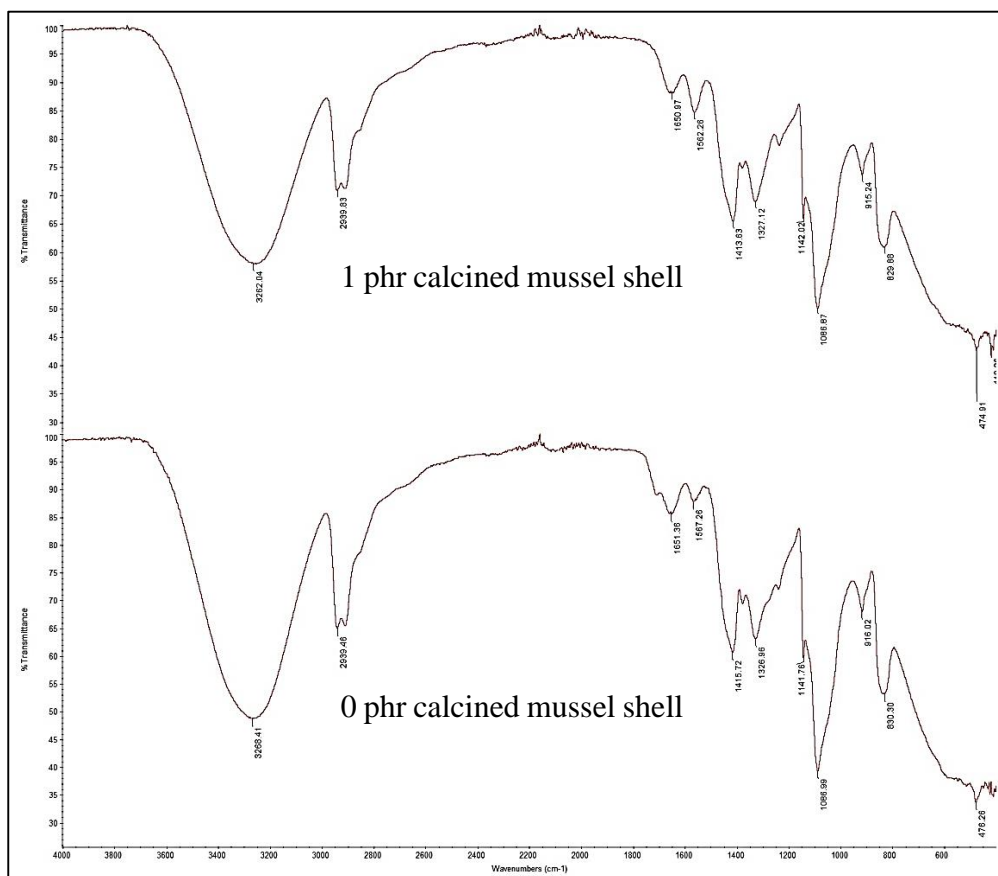
(c)

Figure 4.10 FTIR Spectrum of PVOH composites with different loading level of calcined mussel shell (a) 5 phr and 4 phr, (b) 3 phr and 2 phr, and (c) 1 phr and 0 phr.

Table 4.5: Wavenumber of hydroxyl group (-OH) and C-H stretching of PVOH composites with different loading level of calcined mussel shell.

Loading level of calcined mussel shell, phr	Wavenumber, cm^{-1}	
	O-H Stretching	C-H Stretching
0 phr	3268.41	2939.46
1 phr	3262.04	2939.83
2 phr	3254.01	2939.65
3 phr	3335.55	2917.25
4 phr	3331.38	2935.40
5 phr	3329.11	2942.56

4.3   Summary

In this chapter, the results obtained in every characterization test of calcined mussel shell and PVOH/calcined mussel shell composites were presented and the effects of adding calcined mussel shell also had been discussed.

CHAPTER 5

CONCLUSION AND RECOMMENDATIONS

5.1   Conclusion

Mussel shell waste was utilized to prepare the calcined mussel shell by using calcination under high temperature. The composition and properties of the calcined mussel shell was investigated by the SEM, EDX and XRD analysis. Calcined mussel shell was found to consists of calcium oxide by the EDX analysis.

On the other hand, the effect of adding different amount of calcined mussel shell on the mechanical and chemical properties of the PVOH composites also have been studied. The tensile strength of the PVOH composites increased when the amount of calcined mussel shell increased up to 2 phr. This is because of the presence of interfacial adhesion and also the interaction between the PVOH matrix and calcined mussel shell particles provided reinforcement to the PVOH matrix. However, the tensile strength decreased when the amount of calcined mussel shell further increased. Agglomeration of calcined mussel shell particles occurred due to the poor dispersion had weaken the tensile strength of the PVOH composites by reducing bonding interaction between calcined mussel shell and PVOH. Moreover, the Young's modulus of PVOH composites have similar trend as the tensile strength whereas addition of small amount of calcined mussel shell could provide the reinforcement effect while decreased in interfacial adhesion effect due to the agglomeration at high loading level of calcined mussel shell. The elongation at break of the PVOH composites was increased when the amount of calcined mussel shell added increased. Besides that, the morphologies of fractured surface of PVOH composites were investigated by SEM. The cavities can be observed in the PVOH composites with small amount of calcined mussel shell (≤ 1 phr). PVOH composites with greater amount of calcined mussel shell (≥ 4 phr) were found to have poor dispersion of calcined mussel shell particles where the flake like structure was observed. The crystallite size and crystallinity of the PVOH composites increased as the loading level of calcined mussel shell

increased. Furthermore, increased in loading level of calcined mussel shell had no significant effect toward the *d*-spacing and interchain separation of the crystallite structure. On the other hand, the addition of calcined mussel shell into PVOH matrix had weaken the water absorption capability of PVOH composites. According to the FTIR spectrum, the strength of hydrogen bonding in the PVOH composites had increased as the amount of calcined mussel shell increased.

5.2 Recommendations

Due to some limitations on time and equipment, this study could not able to cover wider range of parameters that could provide more information about the characterization. Hence, the recommendations that can be considered for future work are listed as following.

1. Replace the mussel shell with other alternatives raw materials such as crab shell or chicken bone and compare the differences in characterization and performance.
2. Increase the calcination temperature and duration to eliminate any impurities residue and increase the accuracy of results obtained.
3. Perform the thermogravimetric analysis (TGA) and differential scanning calorimetry (DSC) to investigate the thermal properties of the composites.

REFERENCES

Abhilash, M. and Thomas, D. (2017) '15 - Biopolymers for Biocomposites and Chemical Sensor Applications', in Sadasivuni, K. K. et al. (eds) *Biopolymer Composites in Electronics*. Elsevier, pp. 405–435.

Alawam, K. (2014) *Application of proteomics in diagnosis of ADHD, schizophrenia, major depression, and suicidal behavior*. 1st edn, *Advances in Protein Chemistry and Structural Biology*. 1st edn. Elsevier Inc.

Aramwit, P., Siritientong, T., Kanokpanont, S. and Srichana, T. (2010) 'Formulation and characterization of silk sericin-PVA scaffold crosslinked with genipin', *International Journal of Biological Macromolecules*. Elsevier B.V., 47(5), pp. 668–675.

Azzaoui, K., Lamhamdi, A., Mejdoubi, E. M., Berrabah, M., Hammouti, B., Elidrissi, A., Fouda, M. M. G. and Al-Deyab, S. S. (2014) 'Synthesis and characterization of composite based on cellulose acetate and hydroxyapatite application to the absorption of harmful substances', *Carbohydrate Polymers*. Elsevier Ltd., 111, pp. 41–46.

Barui, A. (2018) *Synthetic polymeric gel*, *Polymeric Gels*. Elsevier Ltd.

Bee, S., Liew, S. Q., Ang, W., Lee, T. S., Bee, S. L. and Rahmat, A. R. (2017) 'Interactive effect of calcined eggshell and montmorillonite on the characteristics of polyvinyl alcohol blends', *Journal of Vinyl and Additive Technology*, 24.

Bergström, J. (2015) 'Experimental Characterization Techniques', in *Mechanics of Solid Polymers*. Elsevier Inc., pp. 19–114.

Callister, W. D. J. and Rethwisch, D. G. (2008) *Fundamentals of Materials Science and Engineering*. 3rd edn. John Wiley & Sons, Inc.

Callister, W. D. J. and Rethwisch, D. G. (2010) *Materials Science and Engineering An Introduction*. 8th edn. John Wiley & Sons, Inc.

Chen, S., Shi, Y., Zhang, X. and Ma, J. (2019) '3D printed hydroxyapatite composite scaffolds with enhanced mechanical properties', *Ceramics International*. Elsevier Ltd and Techna Group S.r.l., 45(8), pp. 10991–10996.

Crawford, C. B. and Quinn, B. (2016) 'Physiochemical properties and degradation', in *Microplastic Pollutants*. Elsevier Inc., pp. 57–100.

Davis, J. R. (2004) 'Introduction to Tensile Testing', in *Tensile testing*. 2nd edn. ASM International, pp. 1–13.

Delgado, J. M. P. Q. and de Lima, A. G. B. (2018) *Transport Phenomena in Multiphase Systems*. Springer International Publishing (Advanced Structured Materials). Available at: https://books.google.com.my/books?id=nGRaDwAAQBAJ.

Fombuena, V., Bernardi, L., Fenollar, O. Boronat, T. and Balart, R. (2014) 'Characterization of green composites from biobased epoxy matrices and bio-fillers derived from seashell wastes', *Materials and Design*. Elsevier Ltd, 57, pp. 168–174.

Gilormini, P. and Verdu, J. (2018) 'On the role of hydrogen bonding on water absorption in polymers', *Polymer*. Elsevier Ltd, 142, pp. 164–169.

Gobin, J., Agard, J., Madera, J. and Mohammed, A. (2013) 'The Asian Green Musse Perna viridis (Linnaeus 1758): 20 Years after Its Introduction in Trinidad and Tobago', *Open Journal of Marine Science*, 03(02), pp. 62–65.

Gooch, J. W. (ed.) (2007) 'Polymer', in *Encyclopedic Dictionary of Polymers*. New York, NY: Springer New York, p. 755.

Gupta, N., Kushwaha, A. K. and Chattopadhyaya, M. C. (2012) 'Adsorptive removal of Pb 2+, Co 2+ and Ni 2+ by hydroxyapatite/chitosan composite from aqueous solution', *Journal of the Taiwan Institute of Chemical Engineers*. Taiwan Institute of Chemical Engineers, 43(1), pp. 125–131.

Hassan, C.M., Peppas, N. A. (2000) 'Structure and Applications of Poly(vinyl alcohol) Hydrogels Produced by Conventional Crosslinking or by Freezing/Thawing Methods', *Advances in Polymer Science*, 153, pp. 37–65.

Ji, L., Song, W., Wei, D., Jiang, D., Cai, L., Wang, Y., Guo, J. Zhang, H. (2019) 'Modified mussel shell powder for microalgae immobilization to remove N and P from eutrophic wastewater', *Bioresource Technology*. Elsevier, 284(March), pp. 36–42.

Jose, J. P. and Joseph, K. (2012) 'Advances in Polymer Composites: Macro- and Microcomposites – State of the Art, New Challenges, and Opportunities', in *Polymer Composites*. John Wiley & Sons, Ltd, pp. 1–16.

Kohli, R. (2012) 'Methods for Monitoring and Measuring Cleanliness of Surfaces', in *Developments in Surface Contamination and Cleaning: Detection, Characterization, and Analysis of Contaminants*. Elsevier Inc., pp. 107–178.

Kumar, V., Ali, Y., Sonkawade, R. G. and Dhaliwal, A. S. (2012) 'Effect of

gamma irradiation on the properties of plastic bottle sheet', *Nuclear Instruments and Methods in Physics Research, Section B: Beam Interactions with Materials and Atoms*. Elsevier B.V., 287, pp. 10–14.

Lemos, A. F., Rocha, J.H.G., Quaresma, S. S. F., Kannan, S., Oktar, F. N., Agathopoulos, S. and Ferreira, J. M. F. (2006) 'Hydroxyapatite nano-powders produced hydrothermally from nacreous material', *Journal of the European Ceramic Society*, 26(16), pp. 3639–3646.

Liu, H., Chen, X. F. and Zhou, C. R. (2010) 'Preparation and Properties of Injectable Hydroxyapatite for Bone Repair Materials', *Key Engineering Materials*, 434–435, pp. 590–593.

Luyt, A. S. and Malik, S. S. (2019) '16 - Can Biodegradable Plastics Solve Plastic Solid Waste Accumulation?', in Al-Salem, S. M. (ed.) *Plastics to Energy*. William Andrew Publishing (Plastics Design Library), pp. 403–423.

Macha, I. J., Ozyegin, L. S., Oktar, F. N. and Nissan, B. B. (2015) 'Conversion of ostrich eggshells (Struthio camelus) to calcium phosphates', *Journal of the Australian Ceramic Society*, 51(1), pp. 125–133.

Martínez-García, C., González-Fonteboa, B., Martínez-Abella, F. and Carro-López, D. (2017) 'Performance of mussel shell as aggregate in plain concrete', *Construction and Building Materials*, 139, pp. 570–583.

Mazumder, S., Nayak, A. K., Ara, T. J. and Hasnain, M. S. (2018) *Hydroxyapatite composites for dentistry*, *Applications of Nanocomposite Materials in Dentistry*. Elsevier Inc.

McCluskey, M. D. (2016) *High-Pressure IR*. 3rd edn, *Encyclopedia of Spectroscopy and Spectrometry*. 3rd edn. Elsevier Ltd.

Mondal, S., Hoang, G., Manivasagan, P., Moorthy, M. S., Kim, H. H. Phan, T. T. V. and Oh, J. (2019) 'Comparative characterization of biogenic and chemical synthesized hydroxyapatite biomaterials for potential biomedical application', *Materials Chemistry and Physics*. Elsevier, 228(November 2018), pp. 344–356.

Pan, Y. and Xiong, D. (2009) 'Friction properties of nano-hydroxyapatite reinforced poly(vinyl alcohol) gel composites as an articular cartilage', *Wear*, 266(7–8), pp. 699–703.

Paradossi, G., Cavalieri, F. and Chiessi, E. (2003) 'Poly(vinyl alcohol) as versatile biomaterial for potential biomedical applications', *Journal of Materials Science: Materials in Medicine*, 14, pp. 687–691.

Peak, D. (2013) *Fourier Transform Infrared Spectroscopic Methods of Soil*

Analysis, *Reference Module in Earth Systems and Environmental Sciences*. Elsevier Inc.

Rahman, R. and Zhafer Firdaus Syed Putra, S. (2018) 'Tensile properties of natural and synthetic fiber-reinforced polymer composites', in *Mechanical and Physical Testing of Biocomposites, Fibre-Reinforced Composites and Hybrid Composites*. Elsevier Ltd, pp. 81–102.

Rajeshkumar, S., Bharath, L. V. and Geetha, R. (2019) 'Broad spectrum antibacterial silver nanoparticle green synthesis: Characterization, and mechanism of action', in *Green Synthesis, Characterization and Applications of Nanoparticles*. Elsevier Inc., pp. 429–444.

Rigano, L. and Lionetti, N. (2016) *Nanobiomaterials in galenic formulations and cosmetics*, *Nanobiomaterials in Galenic Formulations and Cosmetics: Applications of Nanobiomaterials*. Elsevier Inc.

Riley, A. (2012) 'Basics of polymer chemistry for packaging materials', in *Packaging Technology: Fundamentals, Materials and Processes*. Woodhead Publishing Limited, pp. 262–286.

Rocha, J. H. G., Lemos, A. F., Agathopoulos, S., Valério, P., Kannan, S., Oktar, F. N. and Ferreira, J. M. F. (2005) 'Scaffolds for bone restoration from cuttlefish', *Bone*, 37(6), pp. 850–857.

Rudnik, E. (2012) *Compostable Polymer Properties and Packaging Applications*. First Edit, *Plastic Films in Food Packaging: Materials, Technology and Applications*. First Edit. Elsevier Inc.

Saba, N., Jawaid, M. and Sultan, M. T. H. (2018) 'An overview of mechanical and physical testing of composite materials', in *Mechanical and Physical Testing of Biocomposites, Fibre-Reinforced Composites and Hybrid Composites*. Elsevier Ltd, pp. 1–12.

Sangwaranatee, N. W., Teanchai, K., Kongsriprapan, S. and Siriprom, W. (2018) 'Characterization and analyzation of chitosan powder from Perna Viridis shell', *Materials Today: Proceedings*. Elsevier Ltd, 5(6), pp. 13922–13925.

Sanyal, M. K., Datta, A. and Hazra, S. (2007) 'Morphology of nanostructured materials', *Pure and Applied Chemistry*, 74(9), pp. 1553–1570.

Sathiyavimal, S., Vasantharaj, S., Oscar, F. L., Pugazhendhi, A. and Subashkumar, R. (2019) 'Biosynthesis and characterization of hydroxyapatite and its composite (hydroxyapatite-gelatin-chitosan-fibrin-bone ash) for bone tissue engineering applications', *International Journal of Biological Macromolecules*. Elsevier B.V., 129, pp. 844–852.

Sharma, S. K., Verma, D. S., Khan, L. U., Kumar, S. and Khan, S. B. (2018) *Handbook of Materials Characterization*, *Handbook of Materials Characterization*.

Siriwardena, S. (2018) *Perna viridis (Asian green mussel)*. Available at: https://www.cabi.org/isc/datasheet/70090#todescription (Accessed: 6 July 2019).

Syed, I., Garg, S. and Sarkar, P. (2018) *Entrapment of essential oils in hydrogels for biomedical applications*, *Polymeric Gels*. Elsevier Ltd.

Thomas, D., Zhuravlev, E., Wurm, A., Schick, C. and Cebe, P. (2018) 'Fundamental thermal properties of polyvinyl alcohol by fast scanning calorimetry', *Polymer*. Elsevier Ltd, 137, pp. 145–155.

Trakoolwannachai, V., Kheolamai, P. and Ummartyotin, S. (2019) 'Characterization of hydroxyapatite from eggshell waste and polycaprolactone (PCL) composite for scaffold material', *Composites Part B: Engineering*. Elsevier Ltd, 173(April), p. 106974.

Tretinnikov, O. N. and Zagorskaya, S. A. (2012) 'Determination of the degree of crystallinity of poly(Vinyl alcohol) by ftir spectroscopy', *Journal of Applied Spectroscopy*, 79(4), pp. 521–526.

Ul-Hamid, A. (2018) *A Beginners' Guide to Scanning Electron Microscopy*, *A Beginners' Guide to Scanning Electron Microscopy*.

Wakai, F. (2013) *Development of Superplastic Ceramics*. Second Edi, *Handbook of Advanced Ceramics: Materials, Applications, Processing, and Properties: Second Edition*. Second Edi. Elsevier.

Zaaba, N. F., Ismail, H. and Mariatti, M. (2016) 'Utilization of Polyvinyl Alcohol on Properties of Recycled Polypropylene/Peanut Shell Powder Composites', *Procedia Chemistry*. Elsevier Ltd., 19, pp. 763–769.

Zhang, Z., Ortiz, O, Goyal, R. and Kohn, J. (2014) 'Biodegradable Polymers', in *Principles of Tissue Engineering*. Fourth Edi. Elsevier, pp. 441–473.